Student thesis series INES nr 305

Is there new particle formation in the marine boundary layer of the North Sea?

Natalia Kelbus

2014

Department of
Physical Geography and Ecosystem Science
Lund University
Sölvegatan 12
S-223 62 Lund

Natalia Kelbus. Is there new particle formation in the marine boundary layer of the North Sea?

Master degree thesis, 30 credits in Atmospheric Sciences & Biogeochemical Cycles.

Department of Physical Geography and Ecosystems Science, Lund University.

Is there new particle formation in the marine boundary layer of the North Sea?

Natalia Kelbus
Master degree thesis in Atmospheric Sciences & Biogeochemical Cycles
March 2014

Supervisor: Adam Kristensson, Lund University

Department of Physical Geography and Ecosystem Science
Lund University

Abstract

The effect of aerosol particles on climate and the human health emphasizes the necessity to focus on the research about aerosol particles. Aerosol particles emitted due to anthropogenic activities increase the scattering and absorption of solar radiation in the atmosphere which leads to an increased cooling of the climate (direct effect). In addition, they take part in cloud formation, and thereby they affect the radiative properties of clouds, and an increase in the emission of aerosol particles in general leads to an increasing solar radiation scattering and an alteration of precipitation (indirect effect). Aerosol particles emitted directly to the atmosphere through natural or anthropogenic processes are called primary aerosol particles. Secondary aerosol particles are formed after gas to particle conversion. New particle formation (NPF) mechanism is one of the important secondary aerosol particle sources. The newly formed particles have the ability to grow to cloud activation sizes after processing in the atmosphere, and hence are important for the indirect climate effect. There are still many discussions about the theories describing nucleation process and conditions favorable for NPF, but not a single theory can be regarded as correct yet. However it is known that such components as SO2, NOx, Biogenic volatile organic compounds (BVOC), other organic compounds, and NH_3 are important gaseous precursors in the NPF process. NPF events have been detected at many sites at different environments but there is no information about NPF events detected over the North Sea or over other polluted marine atmospheres. The aim of the study is to investigate whether there are NPF events over the North Sea, how frequent they are, and to identify geographical positions of the NPF events over the North Sea using the newly developed NanoMap method. The Nano Map method requires only the aerosol particle size distribution data, and air mass back trajectories from Hysplit model. For this investigation a size distributions of nano-particles were measured with the Air ion spectrometer (AIS) instrument for particles 2 – 40 nm diameter, and with the scanning mobility particle sizer (SMPS) instrument for particles 10 - 300 nm diameter during March – May 2012 at the Danish North Sea coast field station Høvsøre. This data was combined with data measured 2010-2011 at the Cabauw field site in the Netherlands and data measured 2009-2010 at the Birkenes field site in Norway. The NanoMap analysis showed that there are NPF during 27% of the days at Høvsøre and that the aerosol particles are formed close to or along major shipping lanes. Hence, SO_2 from ship emissions is a possible source of NPF over the North Sea. However, also continental air pollution, continental BVOC emissions, and volatile organic carbon (VOC) emissions from oil stations at the North Sea can be contribution to NPF.

Acknowledgements

I would like to express my special thanks of gratitude to my supervisor Adam Kristensson, Assistant Professor, Dept. Of Physics, Lund University, Lund, Sweden for giving me opportunity to take part in this project and for his continuous support throughout the thesis. I would like to thank Hanna Manninen, University of Helsinki, Finland for Matlab code for AIS data.

Table of contents

1. Introduction and aim

In light of the concerns about global warming, better understanding of aerosol particle effects on climate is needed. According to the IPCC report, anthropogenic aerosol particles influence significantly the energy budget of the earth, but the value of the radiative forcing has the highest uncertainty among all atmospheric cooling and warming agents (IPCC, 2013, Figure 1). Among the most important reasons for the high uncertainty is the lack of proper quantification of aerosol particle sources, the fate of atmospheric particles, their radiative scattering properties, and the microphysical process of cloud formation.

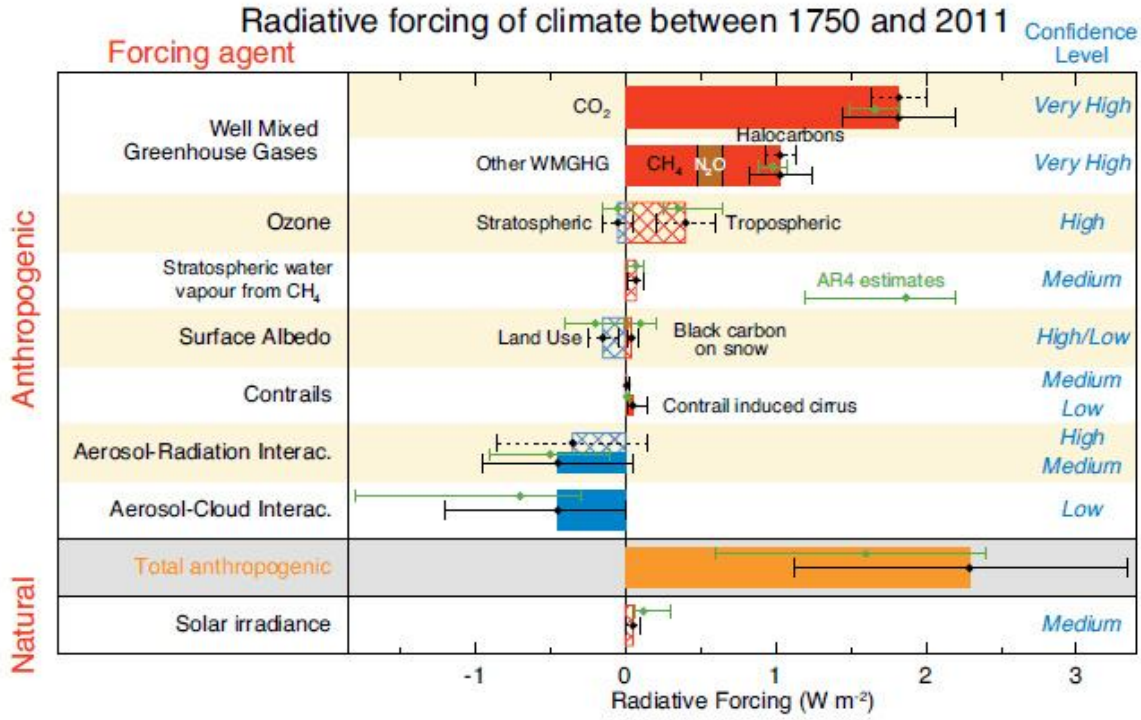

Figure 1: Components of the radiative forcing of the climate induced by human activities and natural processes. A positive radiative forcing is defined as the extra amount of energy trapped in the earth-atmosphere system due to different components. A positive radiative forcing leads to a warming and a negative to a cooling of the climate. Solid bars represent affective radiative forcing of complex forcing agents that entail quick change of some components of the atmosphere. Hatched bars show radiative forcing. The thin black lines at the bars show the uncertanty of the effective radiative forcing, green lines represent uncertainties for radiative forcing value from previous IPCC. (Reproduced from IPCC Fifth Assessment Report: Climate Change 2013, IPCC, 2013).

Aerosol effects on climate are usually described as a direct and an indirect aerosol effect. The direct aerosol effect describes how aerosol particles scatter and absorb incoming solar radiation. Conversely, the indirect aerosol effect describes how aerosol particle emissions have altered the influence on cloud formation and thereby the radiative properties of clouds.

Due to the increase of anthropogenic aerosol particles, the number of cloud droplets is also increasing at the same time as the size of droplets is decreasing. According to the first indirect effect, cloud albedo will increase as a consequence of this process (Haywood and Boucher, 2000). The second indirect effect comprises the way in which aerosol particles affect clouds properties and thus precipitation patterns. The increasing cloud droplet concentration will likely result in a reduction of precipitation rate and an increase of cloud lifetime (Haywood and Boucher, 2000).

IPCC (2007) has estimated that, in total, the net radiative forcing due to the direct and first indirect effect is -1.3 W m^{-2}, although the uncertainty is very large (Figure 1).

In addition to climate, aerosol particles affect human health. There are number of studies showing that particulate matter can cause different types of chronic diseases. Depending on the size of the particles they can penetrate deep into the lungs and cause a number of respiratory and cardiovascular diseases, affect central nervous system, and so on (Pope and Dockery, 2006). The cardiovascular diseases may even cause premature mortality.

There are many sources of particles in the atmosphere, both of natural and anthropogenic origin, which can both directly support new particles to the air ("primary aerosol formation"), and indirectly via gas-to-particle conversion ("secondary aerosol formation"). One of the very important secondary particle sources, especially as regards to global particle number concentrations, and the indirect climate effect, is the mechanism entitled "new particle formation" (NPF). During these new particles formation events, a large pool of new nano-meter sized particles is formed in the atmosphere. These are able to grow by condensation of gas-phase species to sizes relevant for cloud droplet formation, to so called "cloud condensation nuclei" (CCN) (Kristensson, 2013).

New particle formation events and growth of the particles have been detected in different environments of rural, urban and remote marine character (Holmes, 2007). A number of studies have been conducted to identify different mechanisms of particle formation, the source of particles and conditions favorable for nucleation events. For example, analysis of eight years data of size distributions at a boreal forest at Hyytiälä showed that new particles are formed frequently during spring and autumn months, less in summer and minimum in winter (Dal Maso et al., 2005). In this environment, biogenic organic compounds are mainly responsible for the growth of the nano-particles to cloud-relevant sizes.

While the NPF events over continental boundary layers are frequent, few events are detected over pristine marine boundary layers (Weber et al., 2001). However, over polluted sea areas, like the North Sea, the Mediterranean, the Gulf of Mexico, Chinese Sea, and so on, we expect that the marine boundary layer (MBL) contains a mix of ship emission and continental pollutants that might favor NPF events. Indirect evidence exist that such events occur in the MBL of the North Sea (Kristensson et al. 2008). On the other hand, no studies have been conducted that support the circumstantial evidence. Although there is evidently NPF events occurring over the MBL in the Baltic Sea (Hyvärinen et al., 2008), this sea is however too strongly influenced by continental emissions due to the proximity to land areas and can be regarded as a sea with continental aerosol particles and not as a sea with marine particles. Nonetheless, further investigations with a better quantification of NPF over the Baltic Sea marine boundary layer and the reasons for NPF are also encouraged.

If NPF events are frequently occurring over ship lanes due to the SO_2 emissions, then NPF events will be significantly upgraded as one of the most important, maybe even dominant contributors to CCN globally. Hence, this issue is one of utter importance to investigate for a better understanding of anthropogenic aerosol particle radiative forcing.

The aim of the given study is to:

1. Investigate if particle formation events exist over a polluted sea, in this case the North Sea. Measurements of the particle number size distributions are performed along the Danish North Sea coast-line for this objective. Also available data from coastal near sites in the Netherlands and in Norway are used for this purpose.

2. Find out how often the events occur over the North Sea marine boundary layer.

3. Use the NanoMap methodology from Kristensson et al. (2014) to estimate with high spatial resolution the position where particles of 1.5 nm diameter were formed during the NPF events over the North Sea.

4. Investigate if they have a prevalence to occur in the vicinity of frequented ship lanes, since SO_2 emitted by the ships is a large contributor to sulphuric acid regionally, which could be a driving force for new particle formation.

2. Aerosol particles in the atmosphere

2.1 The Atmospheric particles and their sizes and sources

By definition, an aerosol is a gas with solid or liquid particles suspended in the gas (Hinds, 1999). The particles in the aerosol are called aerosol particles. There are many aerosol particles of different size, shape and chemical composition in the atmosphere originated from a variety of sources. Aerosol particles properties depend on the size of particles.

Depending on the formation process, aerosol particles are usually described as primary or secondary aerosol particles (Seinfeld and Pandis, 2006). Both types of particles can have human induced and natural sources. *Primary aerosol particles* are emitted directly to the atmosphere usually as a result of mechanical generation or combustion.

For example, sea salt aerosols are produced due to action of wind on the sea surface, when tiny bubbles are formed in “whitecaps” and after bursting of the bubbles, particles of salt are introduced into the air. Another primary production is mechanical grinding. One example of this process is the generation of asphalt particles due to the interaction between road asphalt and the tires of a motor vehicle. The aerosol particles are formed due to the road abrasion and the action of wind making the generated particles airborne. In addition to the mentioned processes, particles can be formed out of dry soil due to the action of the wind over agricultural soil. The size range of the mechanically generated particles varies from few hundred nm to several μm (Kristensson, 2013).

Primary aerosol particles are formed during the first seconds after combustion of fuel in car engines exhaust, in chimneys after wood combustion, etc (Kristensson, 2013). Hot vapors after combustion of fuel enter into the exhaust system and after being cooled in the atmosphere they condense forming new particles with diameters around 10 nm. There are also soot particles formed already in the combustion bed during wood combustion or in the engine of vehicles.

Secondary aerosol particles are formed during gas to particle conversion in the atmosphere and condensation of gases on pre-existing particles (Seinfeld and Pandis, 2006). New nanometer sized particles are formed during gas to particle conversion, whereas the condensation can take place on all size ranges of the pre-existing particles. While the gas to particle conversion is creating a new pool of particles in the atmosphere, condensation is only giving an increased mass of particles, but not any new particles. The sources of the gas emissions that lead to secondary aerosol particles are the following: combustion, biogenic plant emissions, agricultural emissions, etc.

The sizes of atmospheric aerosol particles vary from 1 nm to 100 μm. Airborne particles significantly larger than 100 μm quickly settle to the ground due to gravity, that is why they are not by definition aerosol particles.

Aerosol particles can be classified with respect to their size as Fine particles (1 nm - 1 μm particle diameter) and Coarse particles (1 μm - 100 μm particle diameter). The Fine particles are divided in turn into a Nucleation mode (particle diameters smaller than 25 nm), an Aitken mode (25 nm – 100 nm particle diameter) and an Accumulation mode (100 nm – 1 μm particle diameter) (Kristensson, 2005).

A summary of primary and secondary aerosol particle sources, possible processes giving rise to the different particle types and in which size range the aerosol particles are found is presented in Table 1.

Table 1. Important primary and secondary aerosol particles: sources and formation processes and relevant size ranges for the different aerosol types.

Formation process	Source	Process of introducing particles to atmosphere	Mode
Primary Natural	Mineral aerososol	Wind suspension, surface abrasion	Coarse
	Sea spray aerosol	Wave breaking and bubble bursting	Coarse
	Biogenic aerosols	Abrasion of leaves, microbes, pollen	Coarse
	Organic aerosols	Burning of vegetation	Fine and Coarse
	Volcanic dust	Eruption of volcano	Fine and Coarse
Primary Antropogenic	Black soot from exhaust	Fossil fuels burning	Fine
	Industrial dust	Grinding	Coarse and Fine
	Organic aerosols	Burning of vegetation, exhaust from combustion	Fine
Secondary Natural	Biogenic emissions	Photoxidation of biogenic volatile organic carbon	Fine
	Nitrate	Oxidation of gases after biomass burning	Coarse and Fine
	Gaseous precursor SO2, H2S	Oxidation of gases after volcanic eruption	Fine
Secondary Antropogenic	Organic compounds	Oxidation of products of combustion	Fine
	Sulphate	Oxidation of products of combustion	Fine
	Ammonia	Agriculture, animal production, sewage	Fine
	Nitrate	Oxidation of products of combustion	Coarse and Fine

2.2 Chemical composition

The chemical composition of atmospheric aerosol particles varies greatly and depends on the source.

Primary mineral aerosol particles generated by wind dispersion or surface grinding mostly consist of mineral materials. The mineral dust particles usually contain clays, metal oxides and carbonates (Kristensson, 2011).

Sea spray aerosol particles are formed during wave breaking, contain organic components from the biota in the ocean and sea salt contained in the sea water (Andreae, 2007).

Primary and natural organic continental aerosol particles are emitted to the atmosphere by vegetation or animals. These particles are composed of pollen, bacteria, spores, viruses or fragments from plants and animals, and belong to the coarse mode except for virus, which may belong to the fine mode depending on virus type. Coarse particles can be originated from vegetation burning and they consist of carbon, ash, unburned parts, whereas the main constituents of fine vegetation burning particles are combinations of organic matter, soot carbon and inorganic species (Janhäll et al., 2010).

Volcanoes should also be mentioned as a considerable natural source of aerosol particles. During volcanic eruptions huge amount of ash particles and the gases SO_2

and H_2S are emitted into the atmosphere (Mother and Pyle, 2003). The different gases are playing an important role as precursor gases for secondary aerosol formation (Mother and Pyle, 2003).

Primary anthropogenic aerosol particles come from combustion, different manufacturing processes, mechanical grinding and other human activities. Both organic and inorganic species can be found in these particles. For example soot particles are directly ejected to the air after fuel burning at the exhaust. There are substantial organic emissions from fossil fuel and biomass combustion. Inorganic species, metals, ammonium, and insoluble minerals are also present in human induced emissions. Metals can be emitted after combustion of fossil fuels, or in the smelting industry. Man-made origins of ammonium in the atmosphere are fertilized lands, sewage and animal husbandry.

The chemical composition of the secondary aerosol particles is represented mainly by sulfates, nitrates and organics.

One of the biggest natural sources of organics for secondary aerosol production are biogenic volatile organic compounds (BVOC) emitted by vegetation, for example terpenes. BVOC can be oxidized during daytime in the atmosphere and form secondary organic aerosol particles (Kulmala et al., 2004). BVOC and sulfuric acid could either condense on existing aerosol particles in the air, thereby increase the mass concentration of particles (see section 2.3), or lead to the formation of new particles (see section 2.6).

Gaseous sulphur dioxide originated form fossil fuel burning or volcano eruptions can be converted to sulfuric acid through atmospheric oxidation, and then condense on the aerosol particles as explained in section 2.3. NO_2 that appears in the atmosphere after fossil fuel combustion can be oxidized to HNO_3 and further react with ammonium to form ammonium nitrate in the aerosol particles (Mother and Pyle, 2003).

2.3 Transformation of aerosol particles in the atmosphere

The following processes are responsible for increasing the size of fine particles during long range transport in the atmosphere: coagulation, and condensation.

Coagulation is a process when particles bump against each other, forming larger particles with a decrease in the number concentration. Such effects like Brownian motion, turbulence, gravity and electrical forces can cause coagulation. The growth effect of coagulation is small, since generally coagulation takes place mainly between relatively small and large particles, and hence the small particles are increasing the mass of the larger particles in a minor way. The loss of particles is more important.

Condensation is more important for the growth of particles. There are semivolatile or reactive vapors in atmosphere that can condense on existing small particles increasing their size. For example, gaseous sulphur acid (H_2SO_4) can be produced from volatile sulphur dioxide (SO_2) by the following reactions (Curtius, 2009):

$$SO_2 + OH + M \rightarrow HOSO_2 + M \quad (R1)$$

$$HOSO_2 + O_2 \rightarrow SO_3 + HO_2 \quad (R2)$$

$$SO_3 + 2H_2O \rightarrow H_2SO_4 + H_2O \quad (R3)$$

where M is chemically neutral molecule that is required for the reaction to proceed.

When the concentration of sulfuric acid reaches a certain level (the gas becomes supersaturated with respect to the concentration at the surface of the aerosol particles), it can condense on existing aerosol particles. Sulfuric acid is an example of a compound that has a very low saturation equilibrium concentration. Hence, most sulfuric acid is found in the particle phase (Curtius, 2009).

After condensational growth, the particles in the Aitken mode have a possibility to reach a size when they can act as cloud condensation nuclei (CCN). CCN are particles approximately 100 nm diameter in size or larger on which water vapor can condense and form a cloud droplet (Kristensson 2013).

As the cloud droplets attain a new chemical composition with more gases condensing on them, the aerosol particles will not achieve the same size as before cloud activation when the cloud droplet evaporates. They will be slightly larger.

2.4 Cloud activation

Cloud condensational nuclei (CCN) are aerosol particles, which can be activated to cloud droplets in an environment where water vapor does not experience any physical barrier for water vapor condensation on these particles. In the absence of aerosol particles in atmosphere we would have no clouds. For homogenous condensation of water vapor for the formation of water droplets, we need a relative humidity of 200% at 20°C, which is not common for natural conditions (Seinfeld at al., 2006). However, not all particles in the atmosphere are CCN and take part in cloud formation. One of the most important properties that the particles must have is the ability to attract water, or in the language of aerosol physicists: they should be hygroscopic. The ability of the particles to attract water molecules depends on the chemical composition and morphology of the aerosol particles and their size.

To understand how water condenses or evaporates from particles it is necessary to introduce the Köhler theory describing the interaction between water and particles (Köhler, 1938). The Köhler theory combines two effects for the water vapor interaction with particles: The Kelvin effect and the Raoult effect.

The Kelvin effect or curvature effect relates the dependence of vapor pressure to the size of the droplet or, in other words, the curvature of the droplet surface. Let us consider a small water droplet surrounded by water vapor. If the water droplet is in equilibrium, the size of the droplet is not changing since the amount of water molecules taken up by the droplet is the same as evaporated from the droplet. The rate of evaporation is increasing with an increase in curvature (or with a decrease in droplet size). In order to keep the curved droplets in equilibrium, a relatively higher concentration of water vapor is necessary, or in other words a higher water vapor pressure compared to a larger water droplet. A large water droplet can be approximated with a flat surface. The Kelvin effect is describing the relationship between the vapor pressure needed to maintain the equilibrium for a curved water droplet, p_K and the equilibrium vapor pressure for a larger droplet (flat surface), p_0:

$$\frac{p_k}{p_0} = \exp\left(\frac{4\gamma M}{\rho RTd}\right) \quad (1)$$

Where:

γ- droplet surface tension,
M- droplet molar mass,
ρ – droplet density
d- droplet diameter
R– gas constant
T- absolute temperature

The ratio is called the saturation ratio. For a larger droplet, this ratio is equal to one. At this point, the rate of evaporation and condensation are equal according to the definition of equation (1). This is also the situation, where meteorologists define 100% relative humidity. Hence, a saturation ratio of one is equal to 100 % relative humidity (RH). When the supersaturation ratio is higher than 1, or alternatively when the RH is higher than 100 %, the rate of condensation is higher than the rate of evaporation. This is referred to as supersaturation. Supersaturation can be given in % analogous to RH, or as a saturation ratio higher than 1 according to the formulism used in equation (1). Equation (1) shows that supersaturation is required for a small droplet to exist as a result of the curvature effect (Figure2).

The Kelvin effect is valid for droplets of only one pure substance, in this case water. But real aerosol particles can contain different impurities in addition to water, and in this case, the Raoult effect should be taken into the account.

The Raoult effect or the solute effect implies decrease of vapor pressure for a droplet in solution with other compounds than water.

For example, if salt particles attract water a solution is formed. The chemical bonds between salt and water in this solution make it difficult for water molecules to evaporate from the droplet. Thus less vapor pressure is needed to keep the droplet in equilibrium. So, these droplets can be in equilibrium with surrounding air at a relative humidity less than 100% because of vapor pressure depression. If RH is increasing the droplet will take up more water molecules, causing an increase of the particle size (Figure 2).

The equation (2) for the Raoult effect can be written as following:

$$\Omega = \frac{n_L}{n_L + j_I \cdot n_S} \qquad (2)$$

Where:

n_L – mol amounts of solution
n_S – mol amounts of solute
j_I - number of dissociation products

In Köhler theory, the effects of curvature and solute effect are combined to describe the processes between water vapor and the aerosol particle (small water droplet) – equation (3).

$$\frac{p}{p_0} = \Omega_I \cdot \exp\left(\frac{4\gamma M}{\rho RTd}\right) \quad (3)$$

According to the Köhler theory, there is critical level of saturation (when RH is a little higher then 100%) after which the particle will abandon the equilibrium state and will rapidly grow beyond the critical radius only limited by the availability of water vapor and transfer into a cloud droplet (Figure 2). The water droplet has surpassed the critical supersaturation and critical size. Below this size and saturation ratio, the water droplet will maintain an equilibrium size defined by the relative humidity in the atmosphere and the left part of the Köhler curve below the critical size of activation.

A CCN is defined by the value of the critical supersaturation for this particular aerosol particle. If the aerosol particle/water droplet is able to activate at a certain supersaturation in the atmosphere, it is a CCN. Those particles, which require a very high supersaturation for activation, are regarded as non CCN. This is normally the case for less soluble or insoluble particles, and/or particles, which are small in the dry state. Smaller particles will experience a weaker Raoult effect due to the small amount of soluble material.

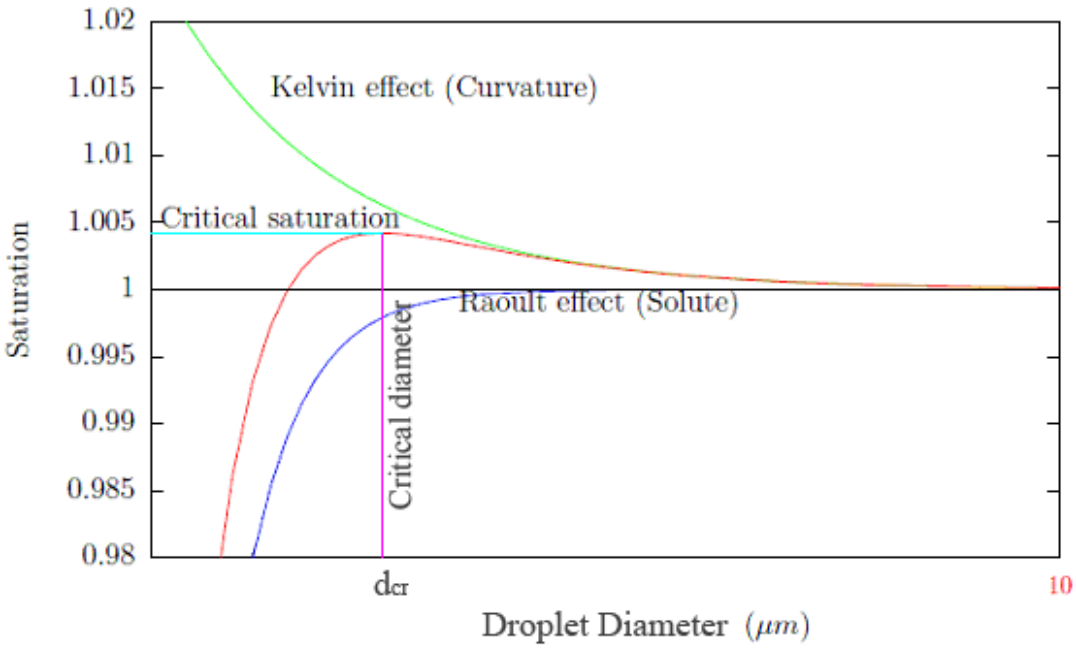

Figure 2. Equilibrium saturation ratio as function of droplet diameter for a specific aerosol particle. The green curve – for pure water, the blue – for a solution droplet (not taking into the account the curvature of the surface), the red – for a solution droplet (adopted from Gunturu, 2010).

2.5 Removal processes

Aerosol particles can reside in the air from days to weeks depending on the size of the particles, chemical composition, meteorological conditions and location. Removal of aerosols from atmosphere can be via wet deposition (wet scavenging), and dry deposition (dry scavenging) (Seinfeld and Pandis, 2006). Deposition can be defined as a process of transportation of aerosol particles from the air to the Earth surface,

with a decrease of the concentration. The majority of the aerosol particles are deposited via wet scavenging.

Wet deposition can take place either in a cloud or below a cloud. Wet deposition in clouds implies that the aerosol particles have been activated to cloud droplets. A minority of the particles have also coagulated with the cloud droplets due to the varying air motion of the aerosol particles compared to the cloud droplets. Aerosol particles might undergo several cloud activation processes and evaporation processes before they are finally raining out as rain droplets. During the activation and evaporation process, the aerosol particles change their chemical composition significantly and become more and more hygroscopic, since condensation of vapors takes place efficiently on the cloud droplets (Seinfeld Pandis, 2006).

In the case of below cloud scavenging, aerosol particles are taken up by precipitation due to collision with falling rain droplets or snow crystals and transported to the Earth surface. This type of deposition is most efficient for particles with diameter larger than 2 μm.

Dry deposition can occur by gravitational sedimentation, interception, impaction, diffusion or Brownian motion (Hinds, 1999). The deposition velocity shows how fast the aerosol particles can reach the surface. This parameter depends on the size of the aerosol particles and the nature of the surface upon which the particles are deposited. Dry deposition is inefficient for aerosol particles in the accumulation mode. As mentioned above, the particles above 100 nm are normally undergoing several evaporation processes before raining out. Particles from accumulation are difficult removed from the atmosphere. Sedimentation is effective for particles with diameters bigger than 4 μm because they are effectively pulled down by the force of gravity. Smaller particles in especially the nucleation mode are effectively deposited due to Brownian motion.

2.6 Atmospheric particle size distributions

The size of the aerosol particles can range from nanometers to micrometers. Usually, the atmospheric aerosol contains a mixture of aerosol particles of different size and shape. To understand how many particles there are of different sizes, it is convenient to present the number concentration normalized with the logarithmic difference between the upper and lower size limit of each size bin of the instrument. It is also convenient to present the particle diameters on a logarithmic scale to observe the several orders of magnitude difference in the particle diameters as in Figure 3 (Hinds, 1999).

Depending on the properties of aerosol particles that are investigated, number, surface or volume distributions with respect to particle size can be presented (Seinfeld and Pandis, 2006). For example, the surface area should be considered if it is necessary to study how aerosol particles interact with lung tissue. The surface area is also important when describing how large surface area is available in the atmosphere for solar light scattering. Since aerosol particles can react with other components in the atmosphere or provide the surface for condensation, it is important to know how large the chemically active surface area is for chemical reactions and condensation.

The volume or mass distribution is useful when describing environmental issues, such as how much mass of soot particles is deposited on the snow or ice which affect the albedo and global warming. The volume distribution is also used to study larger

particles. The mass concentration measurements have been used also traditionally for aerosol particle measurements, also in epidemiological studies. A world-wide network is also available for mass measurements, why continuing to measure volume or mass properties will remain important for a long time to come.

The number distribution is important to characterize when studying cloud formation, since it determines how many aerosol particles can act as CCN (Merikanto et al., 2009). The number of CCN determines the size of the cloud droplets for a given cloud, and thereby it determines the cloud albedo.

Distribution of nucleation, Aitken, accumulation and coarse modes by number, surface and volume concentrations shows that the majority of the particles have diameter smaller than 0.1 μm (Figure 3). The largest fraction of atmospheric aerosol particles belongs to the nucleation mode (Hinds, 1999). The particles of this mode are formed due to new particle formation or combustion and are generally smaller than 20nm. These particles can grow in size after condensation of vapors on them, but they can also coagulate with larger particles if the concentration of larger particles is high, decreasing the concentration in the nucleation mode. If the particles grow due to condensation to sizes above 30nm diameter, they become particles in the Aitken mode. A significant fraction of combustion particles are also emitted in the Aitken mode (Hinds, 1999).

Aerosol particles can grow into the accumulation mode due to condensation of gases in the atmosphere or through cloud processing. As the evaporated cloud droplets end up in the accumulation mode they are often clearly separated from the Aitken mode in their size due to the uptake of condensable species in the droplet phase making the particles larger (Seinfeld and Pandis, 2006).

The volume (or mass) distribution suggests that most mass is normally present in the coarse mode in the atmosphere (Hinds, 1999). These large and heavy particles are mainly produced from mechanical abrasion, such as sea spray, grinding and soil erosion.

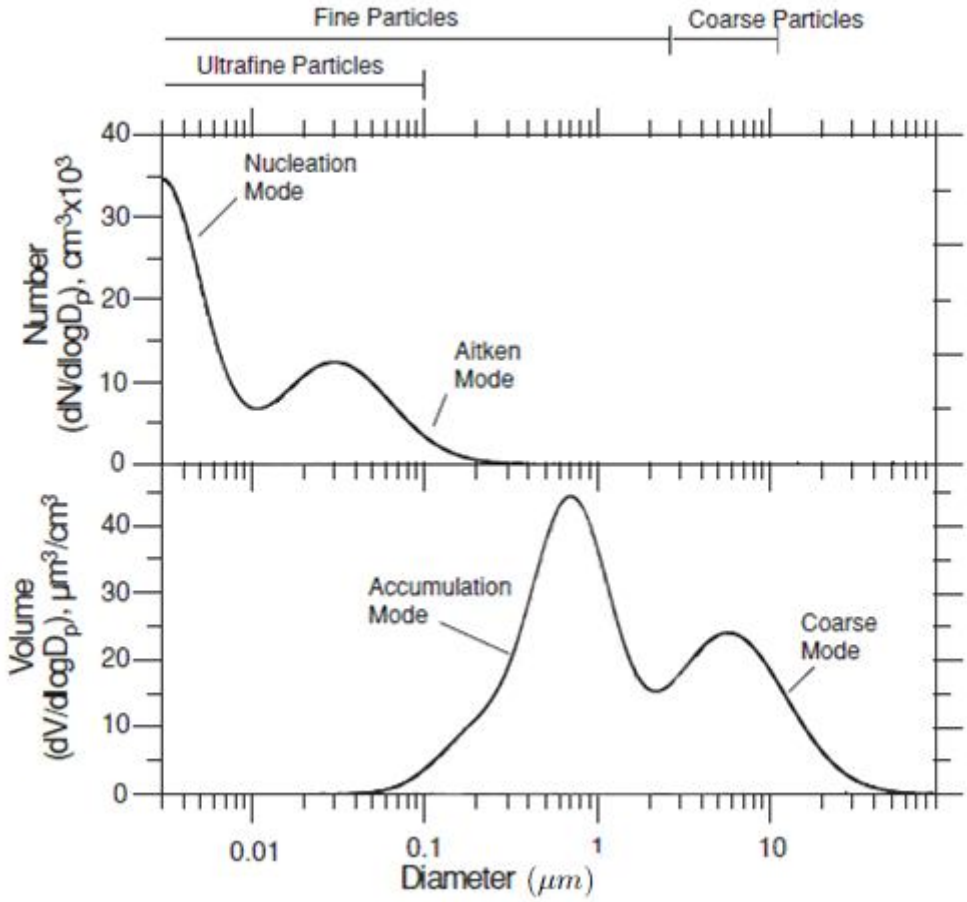

Figure 3. The size distribution of the nucleation, Aitken, accumulation and coarse modes by number and volume concentrations. (adopted from Seinfeld and Pandis, 2006)

3. Nucleation

In the atmosphere, solid or liquid particles of about 1.5 nm in diameter can be formed due to gas-to particle conversion (nucleation). These newly formed particles can be either charged or electrically neutral. This process is called new particle formation, or sometimes nucleation.

Particles of this size are hard to detect by modern instruments until they grow to commonly detectable sizes around 3 to 10 nm. Hence, it is difficult to study the mechanism of formation and there is no certainty yet as to which theories describing the nucleation process are the correct ones, and in which environment they are important.

3.1 Homogeneous nucleation

The classical theory of nucleation is based on fundamental equations of thermodynamics. Several modern theories consider vapor as a substance of single molecules and molecules clusters of different size. These clusters increase their size by bounding single molecules. Most of the air molecules in the atmosphere are single monomers. Due to collisions of the molecules, clusters of molecules are formed but they can be broken down quickly due to evaporation at the same time. An important condition for nucleation to take place is the supersaturation of a particular substance (Curtius, 2009). In saturated air, the number of collisions between molecules is increasing and the gas condenses on suitable surfaces, for example on existing aerosol particles. If there are no pre-existing particles on which vapor can condense, the gas can become supersaturated. In this condition clusters are formed faster and vapor starts to condense on the clusters. This process is called homogeneous nucleation.

3.1.1 Binary homogeneous nucleation

An example of homogeneous nucleation is the condensation of H_2SO_4 and water vapor in the atmosphere. This kind of nucleation is called binary homogenous nucleation, since two components take part in the new particle formation – water vapor and sulfuric acid without any pre-existing particles (Curtius, 2009). In this case the nucleation rate J is dependent on sulfuric acid concentration. However, this process requires special conditions, which are rarely encountered at many sites where NPF have been observed. For example, concentrations of sulfuric acid must be very high in the boundary layer of the atmosphere, otherwise nucleation will not take place. Binary nucleation does not require as high concentrations of sulfuric acid in the free troposphere at low temperature and high relative humidities (Kristensson, 2013). However, also in this environment, the sulfuric acid concentration is often too low for nucleation. No proof exist today that binary nucleation is an important process for NPF in the atmosphere.

3.1.2 Ternary homogeneous nucleation

Ternary homogeneous nucleation theory was suggested as an alternative to binary homogenous nucleation theory. A third component is needed in this theory, and ammonia was suggested as an important compound for the nucleation. The nucleation rate in ternary homogeneous nucleation is also in a strong correlation of sulfuric acid concentrations but lower concentrations are required. The rate of nucleation is much higher at low temperatures and at higher concentrations of

ammonia (Kristensson, 2013). The low temperate is achieved in the upper troposphere. However, concentrations of ammonium are low there, that is why the ternary homogeneous nucleation cannot explain NPF events in many environments alike the binary theory.

3.1.3 Kinetically controlled homogeneous nucleation

The kinetically controlled nucleation theory states that the formation rate of stable clusters depends on the probability and on the rate of two sulfate containing molecules interacting with each other (Kristensson, 2013). The newly formed cluster can be stabilized by other molecules. Since two molecules of sulfate containing clusters are needed for the formation, it means that the formation rate is proportional to the sulfate concentration squared. Since most sulfates is in the form of sulfuric acid, we can approximate the rate with two sulfuric acid molecules as in equation (4)

$$J=K[H_2SO_4]^2 \quad (4)$$

Where:

J - new particle formation rate

K-kinetic coefficient

$[H_2SO_4]$ – sulfuric acid vapor concentration.

Lower concentrations of sulfuric acid are required than in the binary or ternary theory. The power-law dependence of the formation rate with sulfuric acid has been documented in many studies in Europe, that is why this is sometimes a good theoretical model for nucleation (Sipilä et al., 2010). However, it is not expected that nucleation is taking place in this way in the atmosphere. Kulmala et al. (2013) show that a pre-existing cluster surface is likely needed for the nucleation. In this theory there is no cluster before the nucleation as explained in the next section.

3.2 Heterogeneous nucleation

Usually there are clusters already present in the atmosphere of different chemical composition already, so supersaturated vapors condense on existing clusters. This kind of nucleation is called heterogeneous nucleation, condensation occurs on another substance (Seinfeld, 2006).

3.2.1 Cluster activation

One of the heterogeneous theories is the cluster activation theory. According to this theory non-activated clusters in atmosphere become activated after collection of one molecule of sulfuric acid. Other components can also participate in cluster activation, but it is still unclear what components exactly and how they can intensify the nucleation rate (Kristensson, 2013). Since only one sulfuric acid molecule is needed, the formation rate is proportional to the concentration of sulfuric acid:

$$J=A[H_2SO_4] \quad (5)$$

Where:

J - new particle formation rate

A- coefficient

$[H_2SO_4]$ – sulfuric acid vapor concentration.

Equation (5) shows that nucleation rate is in linear dependence of the sulfuric acid concentration. Observations confirm that this is the most likely explanation for nucleation in the boundary layer of a forest (Kulmala et al., 2013).

3.2.2 Ion-induced or ion-mediated nucleation

Another theoretical approach to describe nucleation is ion-induced theory describing nucleation on charged particles. According to this theory condensation of molecules takes place on existing ion clusters, which are more stable and nucleation rate is higher than for neutral clusters. The ion-induced theory explains nucleation rates in the higher free troposphere where the production of ions is higher due to cosmic rays that ionize the air. (Kristensen, 2013).

3.3 Current understanding of nucleation

The research in nucleation is at the moment very intensive. It is assumed that each theory explain nucleation in certain environments. Binary nucleation theory describes well nucleation rates at industrial zones with high sulfuric acid concentrations. Ternary theory predicts nucleation at urbanized places. Cluster activation and kinetically controlled theories explains new particle formation at lower parts of the atmosphere. Ion-induced approach is used in the upper troposphere (Kristensson, 2013).

3.4 Example of nucleation

Figure 4 shows en example of a new particle formation event at Høvsøre, Denmark (see chapter 4.1 for a description of the field station). Newly formed particles with diameters between 1 and 2 nm were detected at 8:00. After subsequent condensation growth, these particles have grown to about as 30 nm diameter at 20:00.

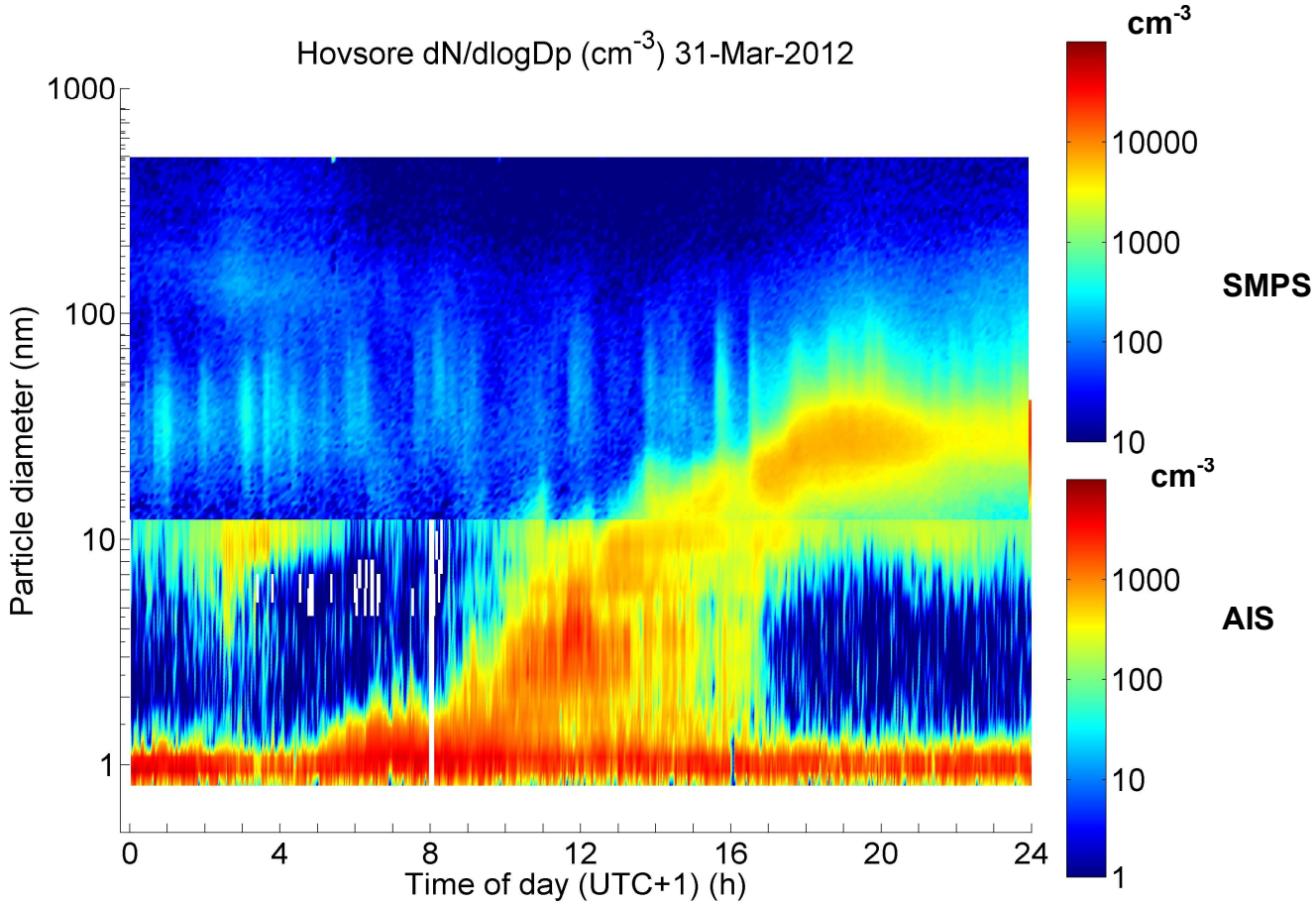

Figure 4. The particle number size distribution March 31, 2012 at the Høvsøre measurement site. In the top panel is plotted the particle number size distribution from the SMPS instrument, while in the lower panel is plotted the distribution from the AIS instrument for the negative ions. The concentration values for the AIS instrument were adjusted for certain sizes to visually fit with the distribution from the SMPS. Hence the absolute values are not correct for the negative ions in all size ranges.

4. Experimental setup

4.1. Site description

In order to study new particle formation events over the open sea a measurement campaign at the coast line of the North Sea was organized between March 9, 2012 and May 31, 2012. The measurements were conducted on the northwest coast of Denmark 1.8 km from the coast-line (56.447 N, 8.152E) at the Test Station For Large Wind turbines, Høvsøre headed by DTU Wind Energy. Measurements of aerosol size distributions were performed with an SMPS (Scanning mobility particle sizer, see section 4.2.) system and with an Air Ion Spectrometer (AIS). The site is at a rural area surrounded by agricultural lands to the east and coast line to the west. The site is flat, without elevation, and open to the winds blowing from the North Sea.

In addition to data from Høvsøre two more data sets from Cabauw (The Netherlands) and Birkenes (Norway) acquired at the ACTRIS database have been analyzed in this study. ACTRIS (Aerosols, Clouds, and Trace gases Research Infrastructure Network) is a European research project that connects several atmospheric research stations into a common network (http://www.actris.net).

The Birkenes measurement site is located in the southern part of Norway at 58º23'N, 8º15'E, 190 m a.s.l, 20 km from the Skagerrak sea, far away from local pollution sources (Asmi et al., 2011). The surrounding lands represent a mixture of forest, grassland, lakes and agricultural lands. Particle size distributions were acquired from a DMPS (differential mobility particle sizer, see section 4.2.) and between July, 10 2009 and June, 26 2010.

Cabauw is a research station in The Netherlands, located to the east of Rotterdam and it is approximately 50 km from the North Sea at 51°58'N, 4°55'E. The surrounding terrain is a flat and open place used for agriculture. Both very polluted air masses from industrialized zones of the Benelux countries and clean air masses from the sea come to Cabauw (Crumeyrolle, et al., 2010). Aerosol size distribution was measured with an SMPS from January, 1 2010 until December, 11 2011.

The characteristics of the instruments used during the three different measurement campaigns in Birkenes, Cabauw and Høvsøre are presented in Table 2

Table 2. Settings of the instruments used at Birkenes, Cabauw and Høvsøre.

	Birkenes	**Cabauw**	**Høvsøre**	
Type of the instrument	DMPS with DMA length 28.5cm. Inner diameter 5cm outer diameter 6.7 cm	Modified TSI 3034 with DMA length 33.3 cm. Inner diameter 1.88 cm Outer diameter 3.92 cm	TSI 3080 SMPS with Long DMA Model 3081	AIS
Time resolution	4 min	5 min	5 min	1 min
Size range measured	15 -550 nm	9-516 nm	12-500 nm	0.5-40 nm
Sheath flow rates	9.21 l/min	4 l/min	5 l/min	60 l/m
Aerosol flow rate	1 l/min	1 l/min	1 l/min	30 l/min

4.2. DMPS/SMPS Instrument

The particle number size distribution can be measured with a DMPS (Differential Mobility Particle Sizer) or an SMPS (Scanning Mobility Particle Sizer) system. Both instruments contain similar components. However, the DMPS is easier to operate than the SMPS system as will be described later in this section. The sample air is scanned in real-time with the DMPS/SMPS system, which consists in series of a drier, a charger, a Differential Mobility Analyser (DMA), and a condensation particle counter (CPC). The system is designed to measure nanoparticles with sizes between a few nanometers to several hundred nm. The scheme of DMPS/SMPS system is presented in Figure 5.

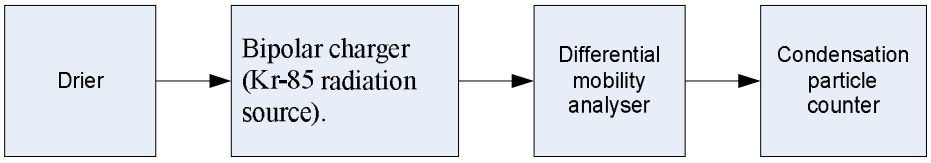

Figure 5. The scheme of the DMPS/SMPS system.

At the fist stage, the aerosol enters the drier, since the standardization of particle number size distribution measurements requires aerosol particles in the dry state. It is easier to compare with other experimental data, if all groups are measuring in the dry state and since the size of the particle can be humidity dependent.

Then, the air is passed through the so called neutralizer, which consists of a Kr-85 bipolar charger. Ambient aerosols particles consist of positively charged, negatively charged and neutral particles in an unknown configuration. After the charger, the aerosol sample obtains a known charge equilibrium state, known as the Boltzmann distribution, with almost equal number of positive and negative particles (Wang et al. 1990). Then, after the charger, the aerosol sample is directed towards the DMA.

In the DMA, particles are separated in accordance to their electrical mobility in the gas flow. Electrical mobility describes the ability of a charged particle to move in the air due to electrical field forces. The DMA works as a size classifier, since a relationship can be obtained between the particle size and electrical mobility:

$$Z = \frac{particle\ velocity}{electrical\ field\ strength} = \frac{np \cdot e \cdot C}{3 \pi \mu D} \quad (6)$$

Where:

Z – particle mobility

np – number of charges

e – elementary unit of charge

μ - viscosity of gas

C – Cunningham slip correction factor

D – particle diameter

As can be seen from equation (6), electrical mobility is inversely proportional to the particle diameter.

The DMA consists of a cylinder with a rod in the centre that normally has a negative charge (Figure 6). A laminar sheath flow of dry air without particles goes into the cylinder. After injection of polydisperse aerosol particles (with different size or mobility) into the DMA, positively charged particles move towards the rod with a velocity, which depends on their electrical mobility. Particles within a certain mobility range are collected in the sample slit depicted as “Monodisperse Aerosol Out” in Figure 2. The rest of the particles are removed via the Bypass flow. By changing the voltage on the rod, a mobility distribution of aerosol particles can be obtained. The relationship between the mean electrical mobility and the geometry of the DMA and the voltage of the inner DMA rod is expressed through the DMA formula. If the Sheath and Bypass flows are equal, the DMA formula becomes (7):

$$Z = \frac{Q_{sh} \ln(r_2/r_1)}{2\pi VL} \tag{7}$$

Where:

r_1 – the inner diameter of the DMA

r_2 – the outer diameter of the DMA

Q_{sh} – sheath flow rate

V – the applied voltage

L – the length of the inner rod

The instrument transfer function expresses what fraction of particles with certain mobility will get into the sample slit of the column at the Monodisperse Aerosol Out flow in Figure 6. The transfer function of the DMA is not sharp, particles with slightly lower mobility, and with slightly higher mobility are allowed to escape through the sample slit in the Aerosol Out flow. The transfer function is ideally triangular in shape, and the width of the transfer function can be described as (Wang and Flagan, 1990):

$$\Delta Z = \frac{Z Q_a}{Q_{sh}} \tag{8}$$

Where:

Q_a – aerosol flow

Hence, for high mobility (or in other words size) resolution measurements it is important to minimize the ratio of the aerosol to sheath air flow rates.

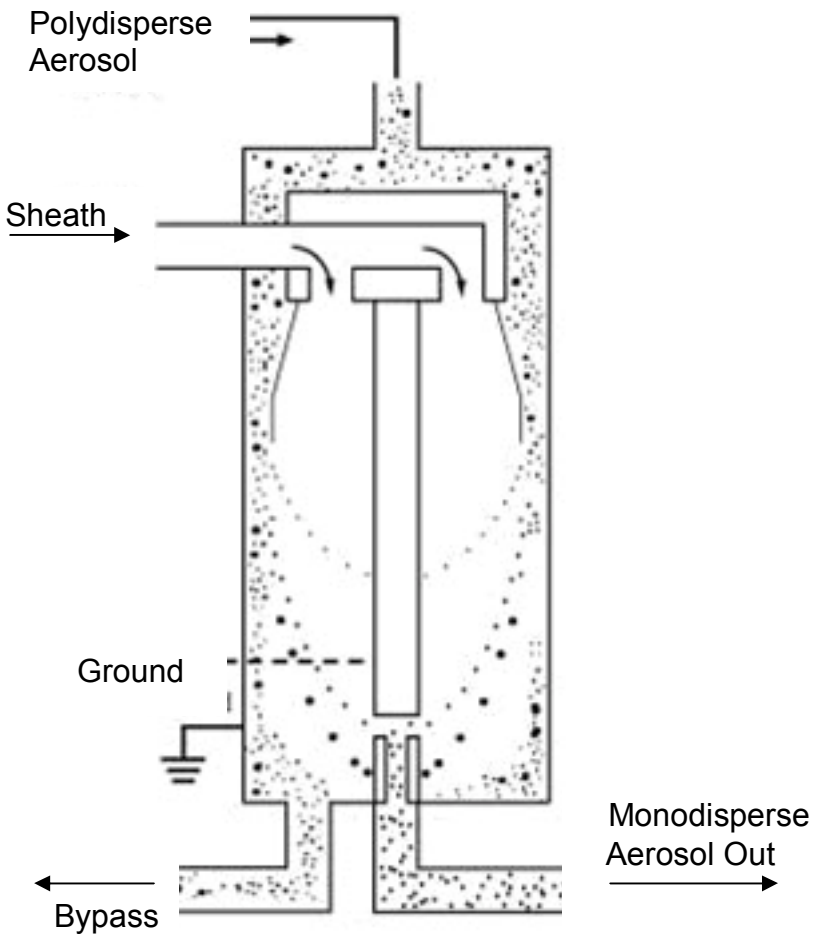

Figure 6. Illustration of Differential Mobility Analyser (DMA). (Adopted from the Operation and Service Manual of a TSI © SMPS 3080 system)

By combining equation (6) and (7) it is possible to obtain the diameter of the particles as function of the applied voltage in the DMA.

When using the DMA in a stepping mode, i.e. by letting the voltage remain constant for a certain time in order to achieve a steady electrical mobility before counting the particles in the CPC, the system is called a DMPS (Differential Mobility Particle Sizer). In this configuration, there is additionally a waiting time to achieve a satisfactory amount of counted particles in the CPC, before switching to a different electrical mobility. With the measurements in this configuration, it takes approximately 5-8 minutes to get a 100 mobility points size distribution (Wang and Flagan, 1990).

In the scanning mode of the DMA, there is no waiting time. Here, the applied voltage on the DMA rod is continuously increasing. Due to the continuous change of the voltage, the mobility of the particles will also vary with time according to changes of the electrical field in the DMA column. In the case of increasing the voltage on the rod, the size of the collected particles in Aerosol Out flow will be increasing compared to the DMA inlet aerosol flow while the aerosol particles are moving through the DMA column. This mode of operation is not as time demanding as the stepping mode. For example, to obtain a size distribution of 100 mobilities, 20-30 seconds are required (Wang and Flagan, 1990). With this mode of operation, the instrument is instead called an SMPS (Scanning Mobility Particle Sizer).

The next step in the DMPS or SMPS instruments is the counting of the particle number concentration with the help of a Condensation Particle Counter (CPC).

The principle of operation of the CPC is based on the detection of scattered laser light by particles moving through a laser beam. In some cases the particles that need to be detected are even as small as 2 nm diameter. Since the laser beam only detects particles larger than 10 μm diameter, these particles need to grow by condensation to this size before they are detected by the instrument (TSI Incorporated, 2002).

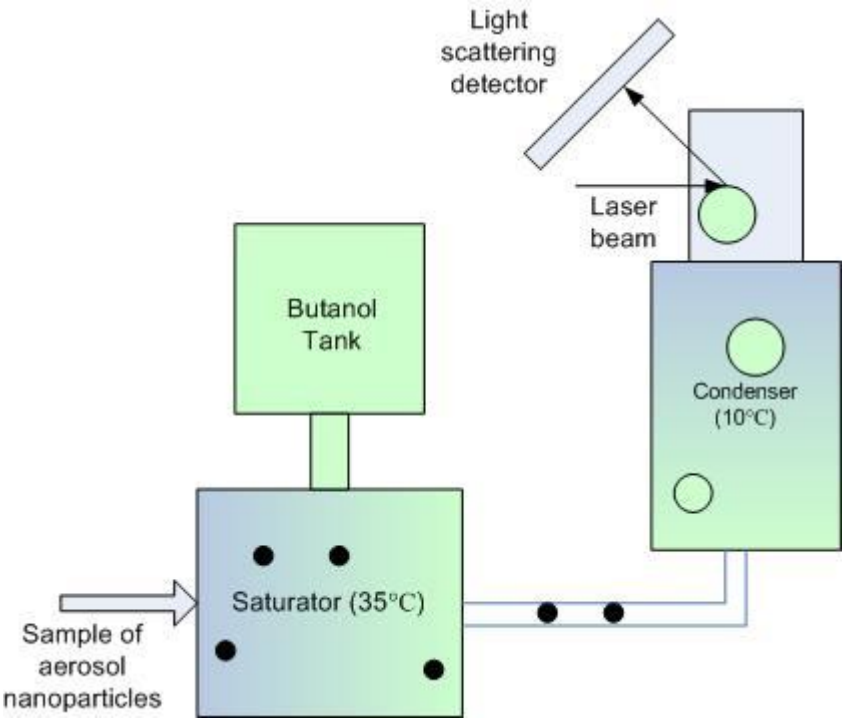

Figure 7. Scheme of the Condensation Particle Counter.

The principle scheme of the CPC is depicted in Figure 7. The monodisperse aerosol flow from the DMA is entering the heated saturation chamber of the CPC where the volume is occupied by a saturated alcohol vapor – normally butanol. In the condenser the sample is cooled and butanol vapor condenses on aerosol particles, thereby increasing their size. After that the droplets pass through the optical sector with the laser beam. The scattered light from the droplet is detected by the scattering photodetector. The light signal from the photodector is converted to an electrical signal and corresponds to one particle. The CPC is counting particles from the DMA and this information is sent to the computer. The computer associates the particle count with the particle mobility deduced by the DMA voltage.

The output data from the DMPS or SMPS instrument are the CPC counts as function of applied DMA voltage and as function of time. To transform this information to particle number size distribution, we must first perform an inversion routine to convert the CPC counts to a mobility size distribution. The mobility distribution can then be converted to a size distribution using the information from equation (6). To perform the computer inversion routine the following parameters are very important: DMA voltage, scan time, bipolar charge distribution, instrument transfer function, CPC detection efficiency curve, CPC and DMA flow, diffusion losses. These parameters

affect the accuracy of the measurements. The transfer function and bipolar charge distribution were explained above, a brief description of the rest of the parameters will be presented below. The DMPS system requires less factors in the inversion than the SMPS system, since the voltage is kept stable for a certain time in the DMPS, so this system is described first.

The counting efficiency of the CPC is increasing with size, and the cut-off size is a diameter at which 50% of particles are detected by the instrument. The efficiency curve is not steep at this point, rather the efficiency is continuously increasing from 0 % efficiency to about 100 % efficiency. The 50% cut-off diameter can vary between 3nm diameter to 20 nm diameter for commercial instruments, where 10 nm is the most common cut-off.

When measuring with a DMPS, particle losses due to diffusion occur. The smaller the particles, the higher the diffusion losses. Thus particle loss correction is also performed in the inversion.

The voltage in the SMPS system is ramped while particles are still in the DMA, or while they are traveling via tubes to the particle counter, and the particles reside some time inside CPC chambers before being counted. Thus the mobility of the particles detected by the CPC corresponds to those particles flowing through the DMA a few seconds earlier. For this purpose time delay parameters called plumbing time (taking into account the residence time in the DMA and tubing, and smearing time (taking into account the residence time in the CPC) are considered (Quant et al., 1992). For example, for the model TSI 3080 CPC and DMA setup that was used in this study for the Høvsøre site, the plumbing time was 1.8 s and the smearing time was 0.9 s.

4.3 AIS Instrument

The Air Ion Spectrometer (AIS) measures in the range between 0.8 nm – 40 nm diameter (Mirme et al., 2007). It provides the size distribution of positively and negatively charged particles with a 5 minute time resolution or better if required.

Alike SMPS systems, the AIS contains DMAs to sample particles according to their electrical mobility. Sample air is sucked into the instrument with a flow rate of 1000 cm^3s^{-1}, and this flow is split between two DMA operating at a flow rate of 500 cm^3s^{-1}. The DMA are supplied with a sheath air flow rate of 1000 cm^3s^{-1}. The AIS does not contain a charger as in the SMPS/DMPS system. The positively and negatively charged central inner electrodes of the two DMA classify naturally charged positive and negative ion clusters or particles respectively (Figure 8). The central rods consist of several parts with different constant voltages to obtain logarithmically and uniformly distributed size fractions (Mirme, 2007). The outer cylinders (Ion-collecting outer electrode) have 21 measuring channels with electrometers. Ions are collected at these sections and the electrical current is measured by electrometers at each channel. A special software processes data from the electrometers, which is inverted to a mobility distribution using the instrument specific parameters and the DMA transfer function.

There are other differences between an SMPS/DMPS and an AIS. The flow rate is much higher in the AIS instrument to minimize diffusion losses of the smallest ion clusters. The dry particle ion size distribution cannot be measured with the AIS during humid conditions since there is no possibility to have a drier in front of the AIS. The

drier would not be effective at the high flow rates, and would additionally remove too many of the smallest clusters due to Brownian diffusion.

The AIS contains a verification system for electrometer current drift. In a separate measurement cycle, a corona charger is charging the particles with opposite polarity, and the remaining particles with the correct polarity are removed by an electrical filter. In this way, only opposite charged particles are reaching the air flow in the DMA column, which are then directed towards the central rod without being collected at the electrometers. In this cycle, it is possible to estimate the noise or the current drift of the electrometers and take this into account in the inversion.

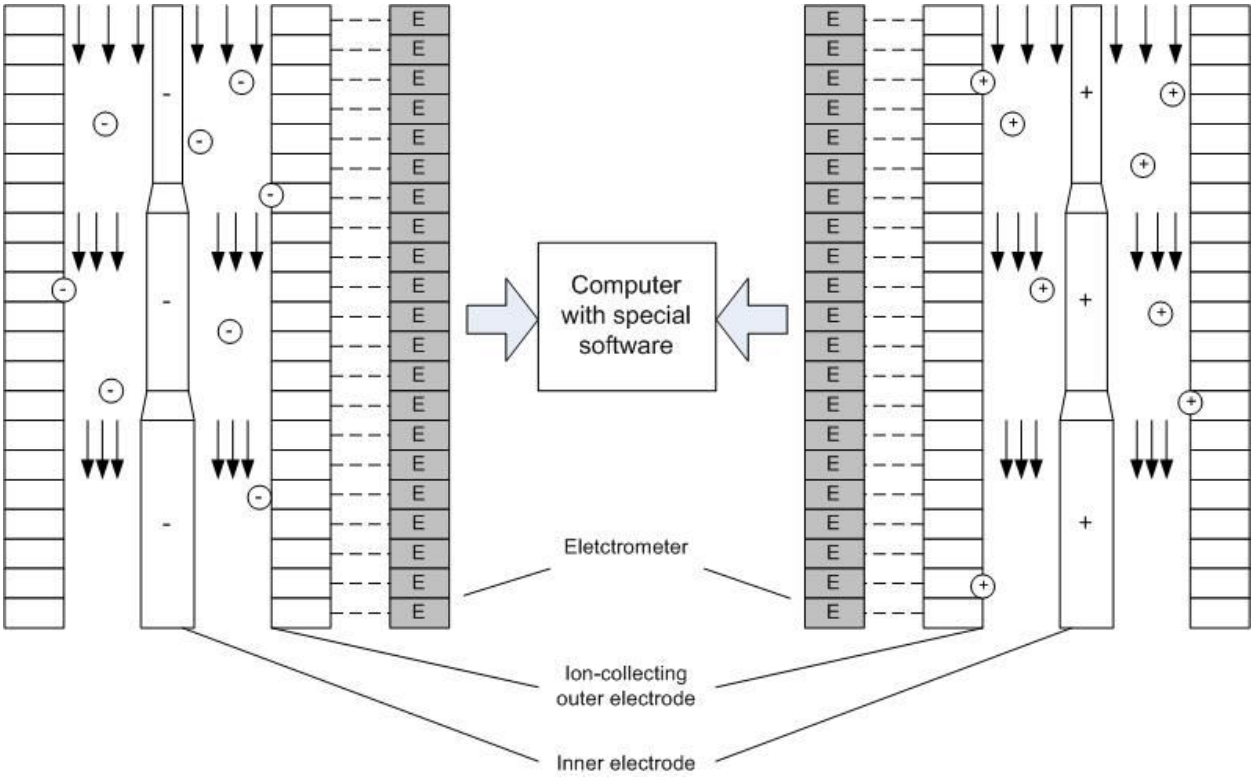

Figure 8. The scheme of the DMA columns of the AIS.

6. NanoMap Method

The NanoMap analysis performed to create maps of where and how often new particle formation occurs around a measurement station contains four different parts:

1. Classification of formation events based on visual inspection of size distribution data.
2. Calculating trajectories from Hysplit model.
3. Calculation of formation events parameters.
4. Creating a map of where particles are formed.

The NanoMap analysis, software, and examples of input and output files needed is presented also at the homepage www.cast.lu.se/NanoMap.htm. The method is also explained in the paper by Kristensson et al. (2014).

6.1. Classification of new particle formation events

Based on a visual inspection of size distribution data for all measured days a classification of NPF can be done. The aim of the classification is to determine days when new particle formation is observed and days without events or unclear data. Dal Maso et al. (2005) elaborated a way to classify NPF events. According to their criteria all days were divided into four classes as described in Table 3.

Table 3: Description of classification classes of New Particle Formation events.

Class	Description
I - Clear event	New particles form in the nucleation mode size range (1.5-25 nm diameter) and grow by condensational growth for at least a few hours. The growth rate can be calculated. The nucleation event has a clear “banana” formed shape that can be seen in the size distribution data plot with time on the x-axis, diameter on the logarithmic y-axis and a surface contour plot of the particle number concentration as function of time and diameter. The event is regionally extensive.
II - Other event	The growth of the particles during new particle formation is terminated or has unclear shape, for example when the event is not regionally extensive. It is difficult to calculate the growth or formation rate.
Non-event	There is no concentration increase observed of particles between 1.5 and 25 nm diameter during any part of the day, except for nucleation mode particles that come from pollution episodes. The nucleation mode particles are usually accompanied by a large Aitken mode population, why it is frequently possible to distinguish pollution episodes from a new particle formation event.
Undefined	It is not clear that the new mode of particles in the nucleation mode is formed as a consequence of new particle formation or if these are particles formed during pollution episodes. Or, it is not clear that we have a nucleation mode growing in size.

Since it is sometimes difficult to assign a class type, and it is very subjective, it is recommended to perform the classification by several different people (minimum 2 people) to avoid the human factor in determining event classes.

Below, in Figure 9 typical examples of new particle formation event classes are shown.

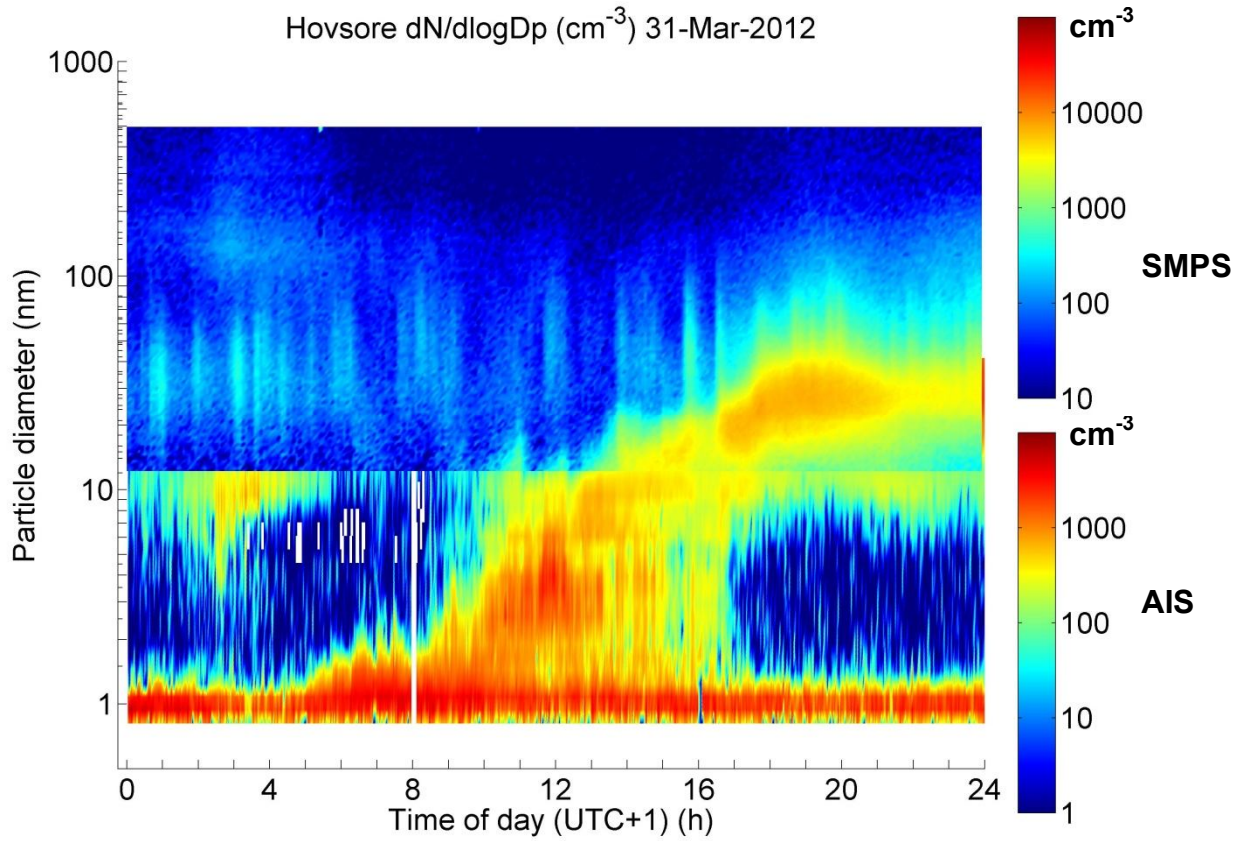

A. Clear event – class I with a “banana” shaped growth.

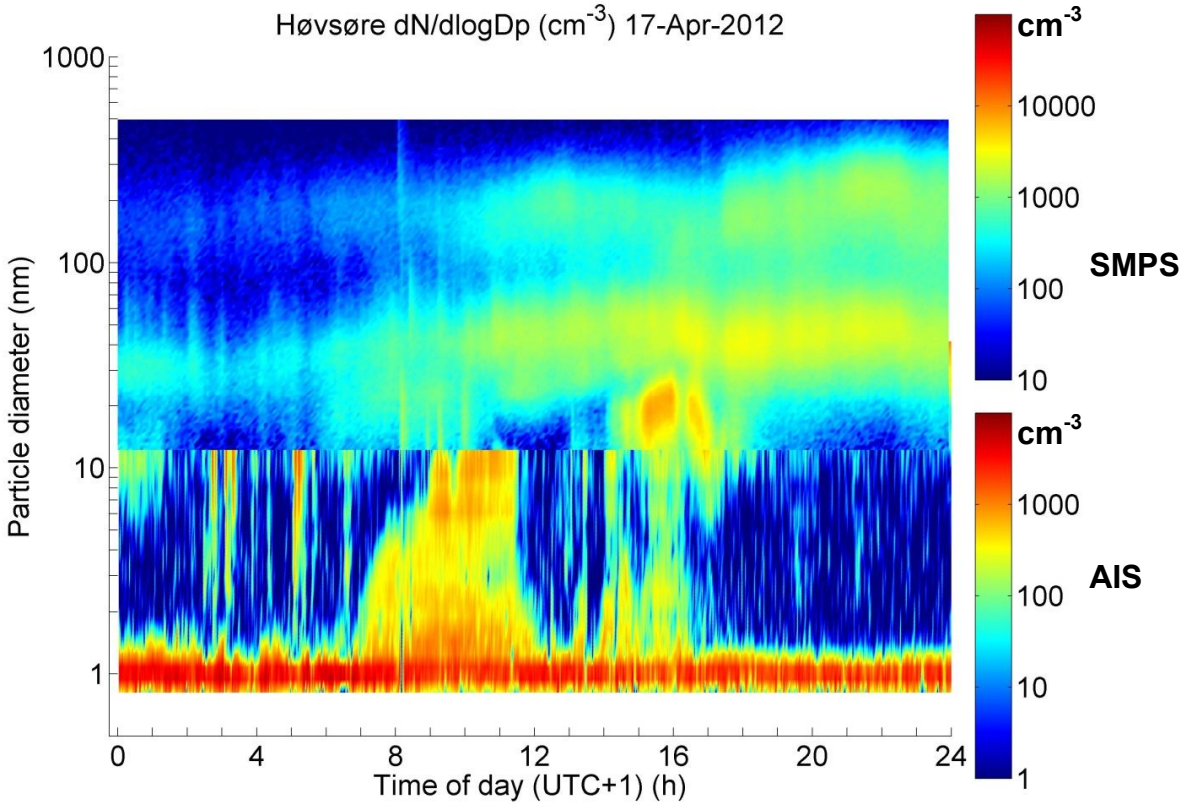

B. A class II event.

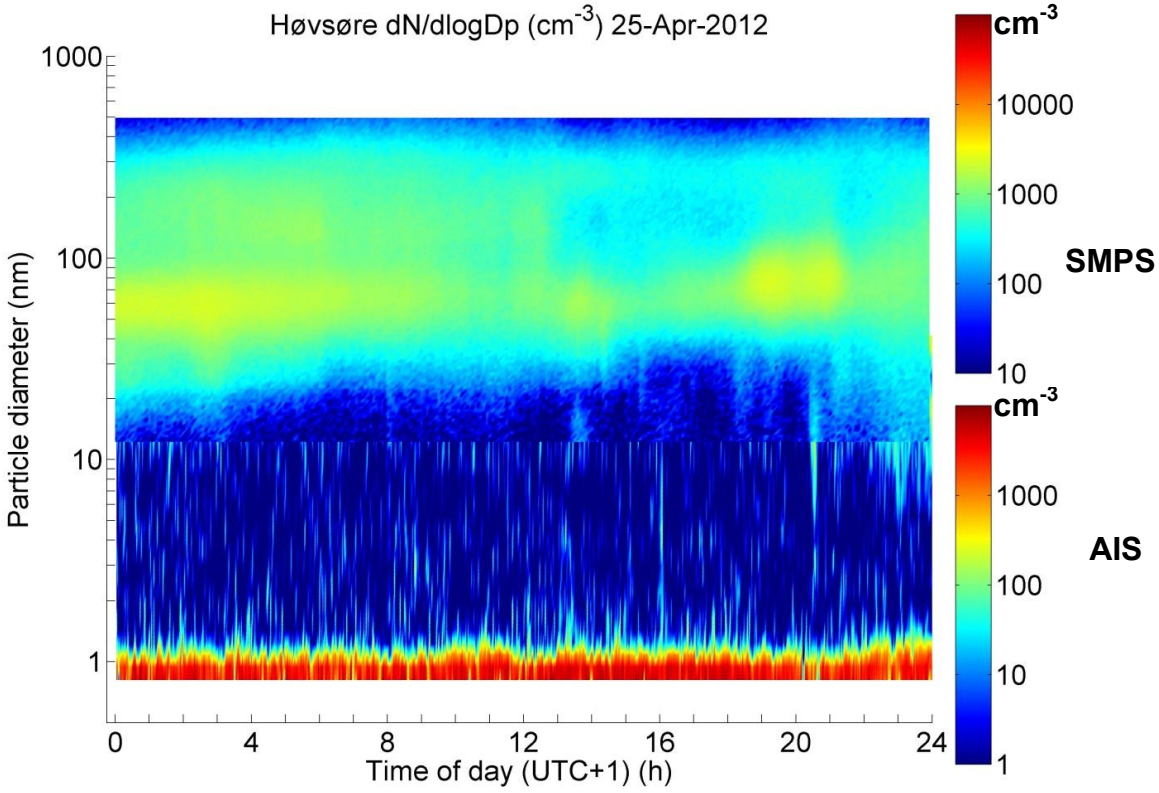

C. Non-event

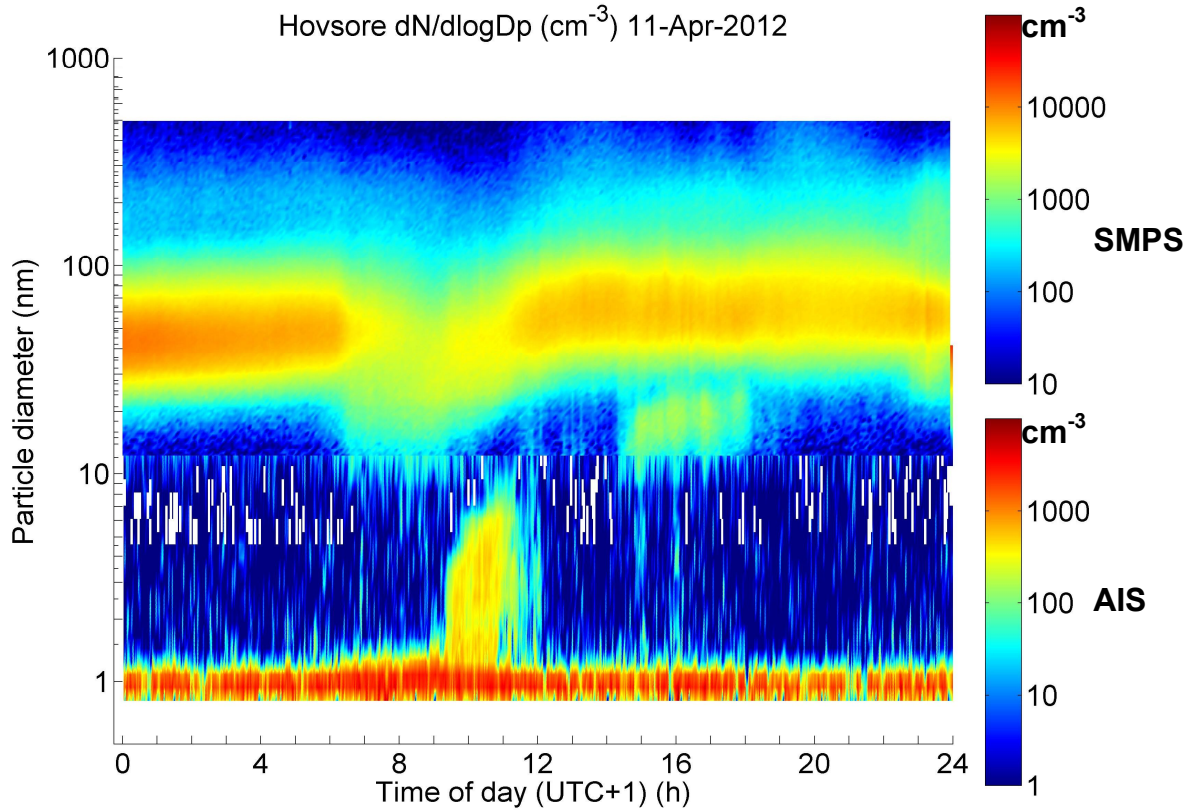

D. Undefined event

Figure 9. The examples of a class I and II event, non-event and undefined event measured 9 March – 31 May 2012 at Høvsøre by SMPS and AIS instruments. Note that the SMPS measures charged and neutral particles, while the AIS graph on the bottom is only for negatively charged particles. The logarithmic concentrations scale (colour) for AIS data were approximately adjusted to visually fit the data from SMPS since negatively charged particle concentrations from the AIS are about 10 times lower than from SMPS. **A**. Class I event (clear event), **B**. Class II event (other event), **C**. Non-event, **D**. Undefined event.

6.2 Calculating trajectories

Aerosol particles measured at the study sites can come from different sources. To identify the origin of the aerosol particles detected by the instruments back-trajectories were used. In this study, they are obtained from the Hysplit (HYbrid Single-Particle Lagrangian Integrated Trajectory) model. The Hysplit model is designed by the National Oceanic and Atmospheric Administration (NOAA) Air Resources Laboratory. It is one of the models that are used in atmospheric research to compute the path of the air mass movement and to simulate the dispersion of pollutants. In this study Hysplit was used to calculate the back trajectories only.

For trajectory simulations, the model requires the following variables: horizontal wind vectors, temperature, height or surface pressure (Draxler and Hess, 1997). The meteorological data as input files can be found at the website http://www.arl.noaa.gov/ready/hysplit4.html.

The model calculates a trajectory line representing movement of a particle in a space during some time when it follows the wind direction (Heinzerling, 2005). Integration of all the positions of the particle will form the trajectory of the air mass. The trajectory

can be plotted on a map. After running the model an output data file is generated that contains information about relative humidity, temperature, pressure, rainfall with varying height along the trajectory, and the geographical position of the air parcel. These data files were used to trace where the formation of 1.5 nm diameter particles took place.

Back trajectories for this study were run for Høvsøre, Birkenes and Cabauw at the starting heights of 100, 500, 3000 meters, with a time interval of 1 hour and the duration of the back trajectories was one week.

The trajectories obtained from Hysplit have uncertainties. The estimated error is 20% – 30% of the distance travelled by the trajectory. Several sources of possible errors can be mentioned: inaccuracy in the input meteorological data, errors in defining starting position, computational errors, and physical errors in representing atmospheric processes in the air (Stohl, 1998).

6.3 Calculation of formation events parameters

All the days classified as Class I – Clear event were further used in calculation of formation events parameters such as Start time (t_start), End time (t_end), End of growth time (EOG).

The start time is the time when the concentration started to increase rapidly above the background concentration at the lowest size bin during a new particle formation event. The end time is the time when the concentration is decreasing again towards the background value. This time is also identified at the lowest size bin. End of growth time is defined as the time when the growing mode of particles formed during a new particle formation event can not be distinguished from the background concentration.

An example of determining the parameters is shown in Figure 10. As can be seen, new particles were detected on the 31 March 2012 at 9.00 (t_start) and the particle burst ended at around 16.30 (t_end) and the growth of the particles lasted several ours. In our case the EOG time is around 1.30 of the next day – 1 April 2012. There are cases when the EOG time is 2-3 days after the start time of the formation.

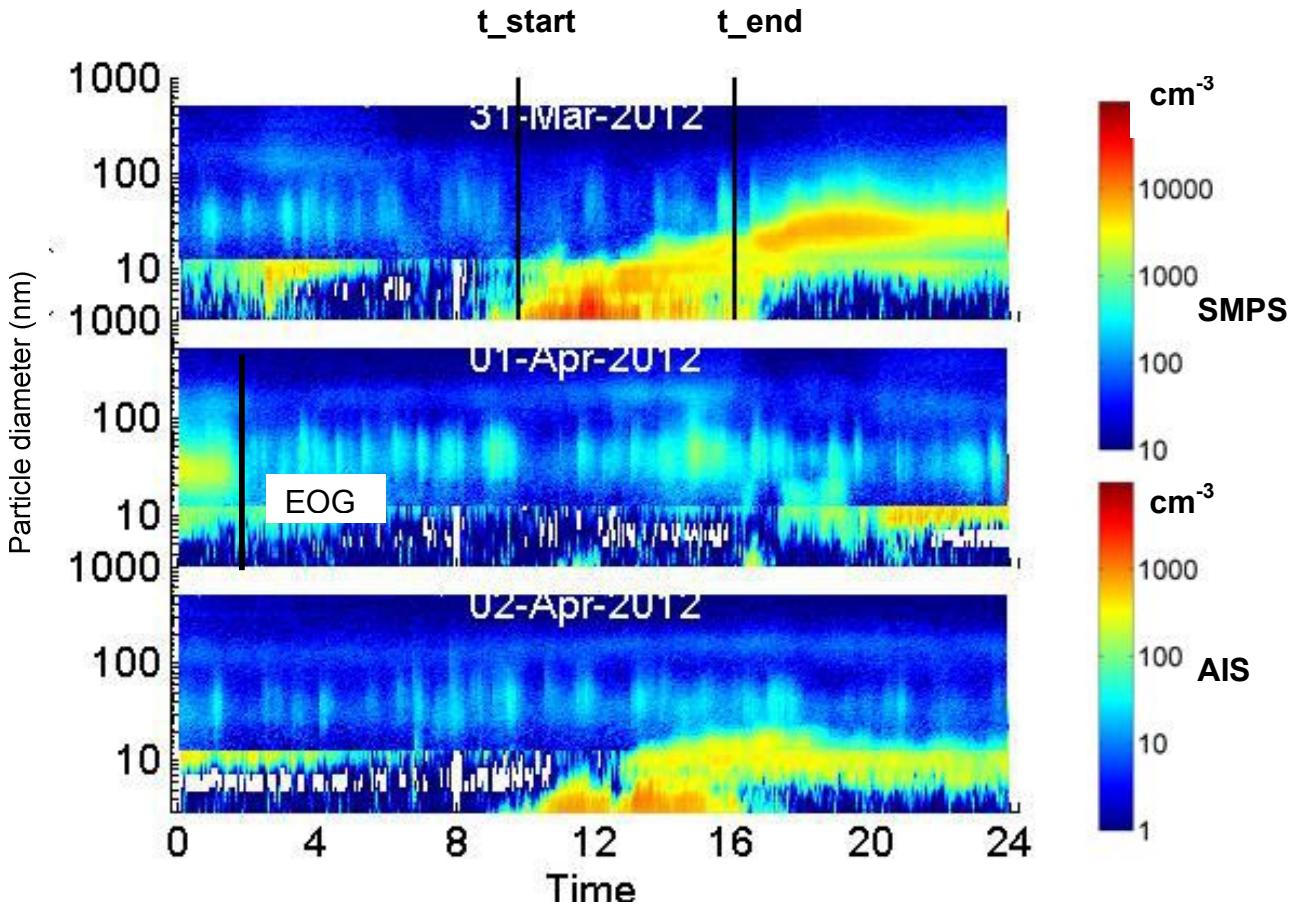

Figure 10. An example of calculated formation event parameters from March 31, 2012 at Høvsøre. Start time (t_start) is 9.00, End time (t_end) is 16.30, End of growth time (EOG) is 1.30 on the 1 April 2012.

Sometimes it is hard to identify an EOG time, since the count median diameter and concentration of the growing mode coincides with the background concentration as in the example if Figure 11. In such cases, a cautious approach has to be adopted, where the selection of the EOG time has to be before the growing mode and background modes merge together.

During a few occasions it is even impossible to select an EOG time, for example when the EOG time is before the ending time of the event. In such cases NanoMap is useless, since it is not possible to attribute formation to any geographical position with the NanoMap method.

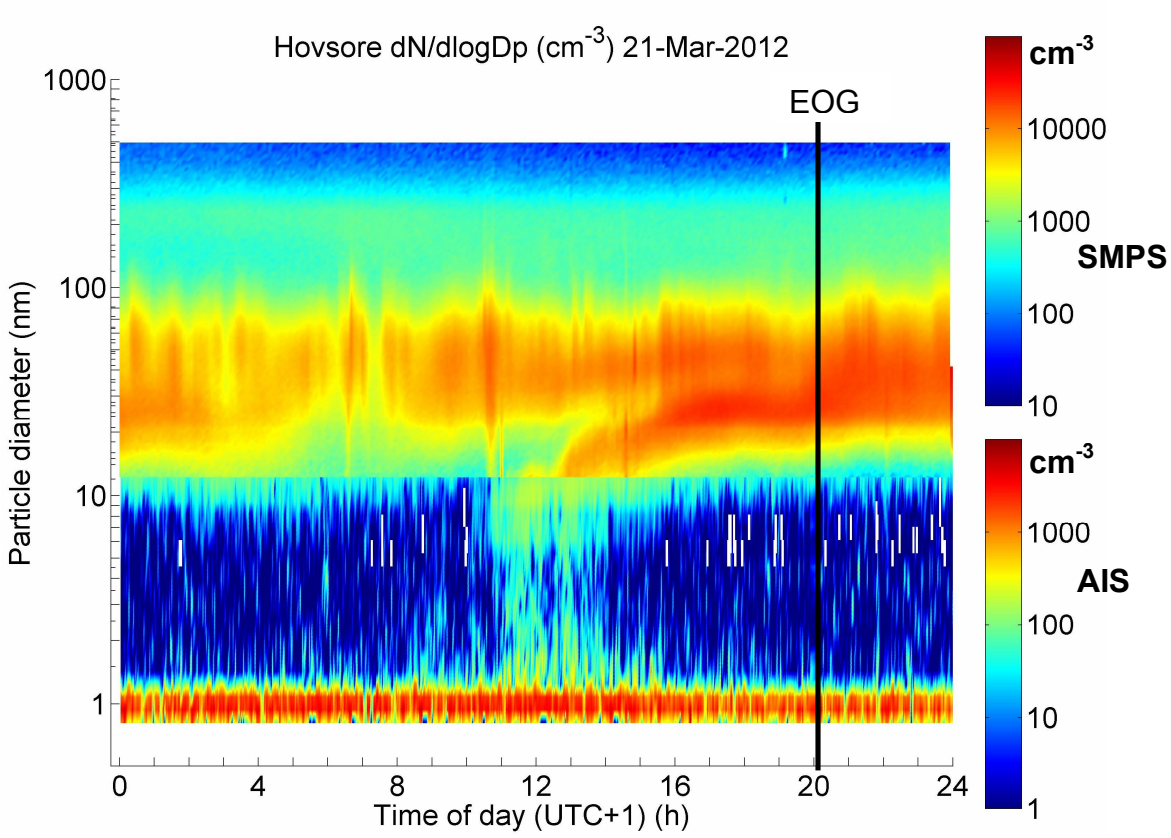

Figure 11. En example of the size distribution plot for 21 May 2012 Høvsøre, when concentration of the growing mode coincides with the background concentration and it is hard to identify the EOG time. The EOG time is defined at around 20.00, before the growing mode and background modes completely merge together.

6.4 Creating a map of new particle formation events

Trajectory output files with data from the Hysplit model together with saved data of t_start, t_end, EOG are used to create a map of the frequency of occurrence of formation events (Kristensson et al., 2014).

According to the method it is possible to identify the geographical point where 1.5 nm particles were formed going backward along the trajectories from the place where the particles were detected at a larger size. For example, at EOG time, in our case at 01.30 on 1 April, the particles grew up to about 40 nm diameter (Figure 10). But these aerosol particles were formed as 1.5 nm at the time frame t_end – t_start, namely 9 – 16 hours ago. By following the back-trajectories 9 – 16 hours backwards in time, it is possible to find the place where the air masses came from and thus to identify the line along where new aerosol particles were formed. Part of the trajectory within the time frame 9-16 hours ago can be plotted on a map (Figure 12).

However it is also possible to analyze the origin of the particles detected 1 hour before the EOG time – at 00.30 on April 1. In this case new particles were formed 8 – 15 hours ago and trajectories will show the location of these particles at that time. Thus the next part of the trajectory will be plotted on the map. By performing this one hour steping from the EOG time until 1 hour after the t_end time, 9 lines in total can be plotted showing where 1.5 nm particles were formed. In Figure 13 we give the example of 5 of these lines, namely the 9 -16, the 8 -15, 7-14, 6 -13, and 5 -12 h ago-

lines. After analyzing all the days when NPF events type I were detected the formation of new particles with a diameter of 1.5 nm will be depicted on the map by lines constituting parts of trajectories of the air masses.

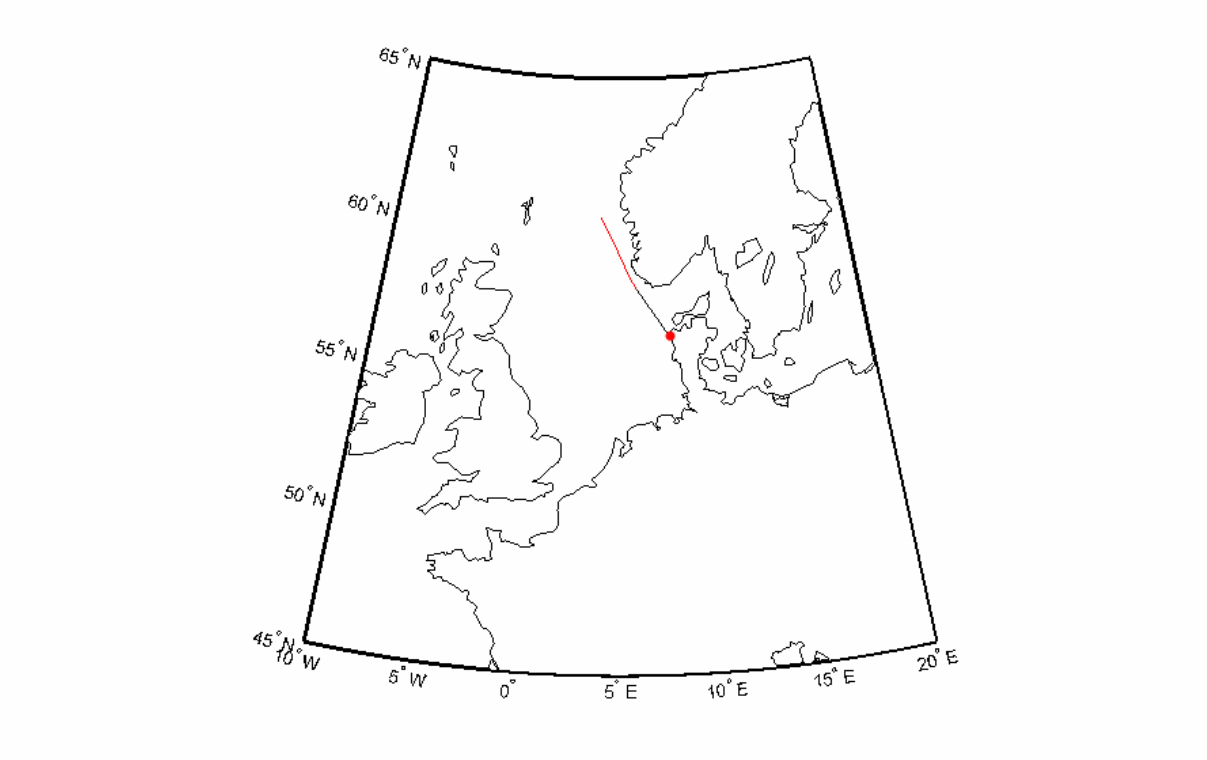

Figure 12. Formation of new particles with diameter 1.5 nm according to NanoMap is depicted with a red line for the growing mode detected on 1 April at EOG time 01.30 for the class I event observed on 31 May 2012 at Høvsøre. The rest of the trajectory is depicted with a black color line.

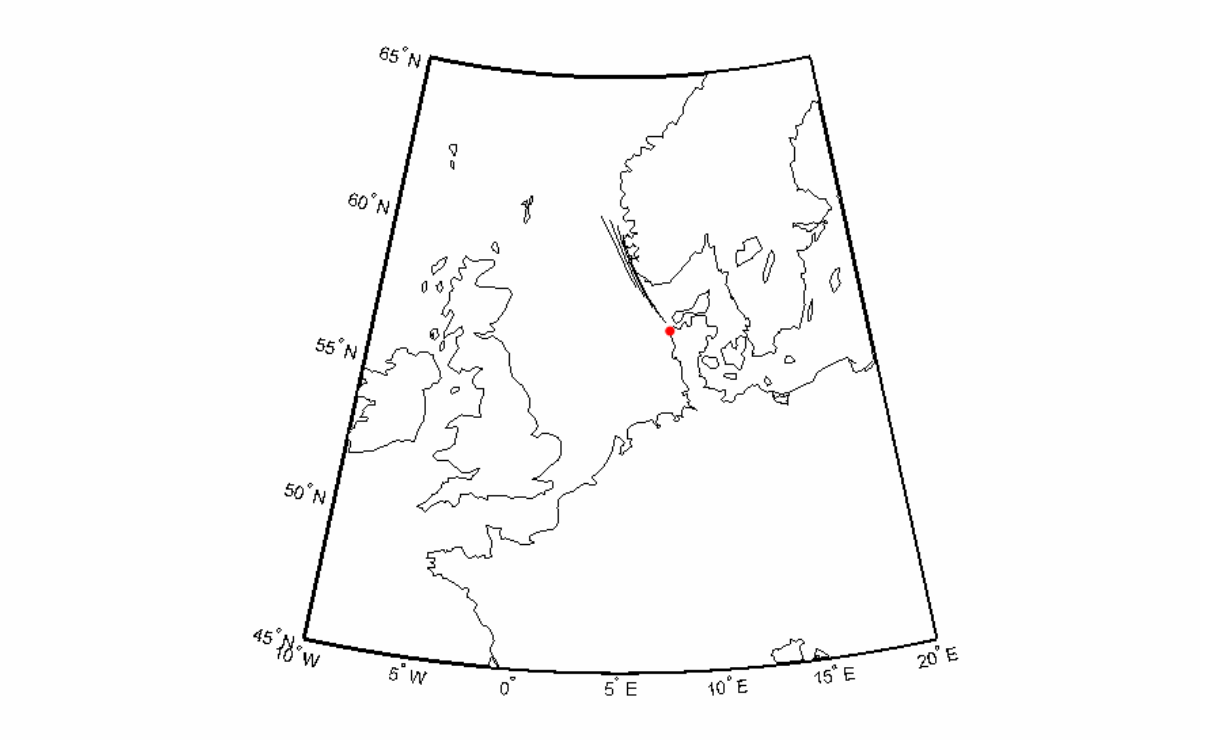

Figure 13. Formation of new particles with diameter 1.5 nm according to NanoMap for the class I event observed on 31 May 2012 at Høvsøre. The red mark represents the location of Høvsøre. Formation of new particles is depicted by black lines constituting parts of the trajectories of the air masses.

In addition to map with lines representing the location of NPF events, it is possible to show also the frequency of the new particle formation as function of grid boxes in the map like in Figure 14.

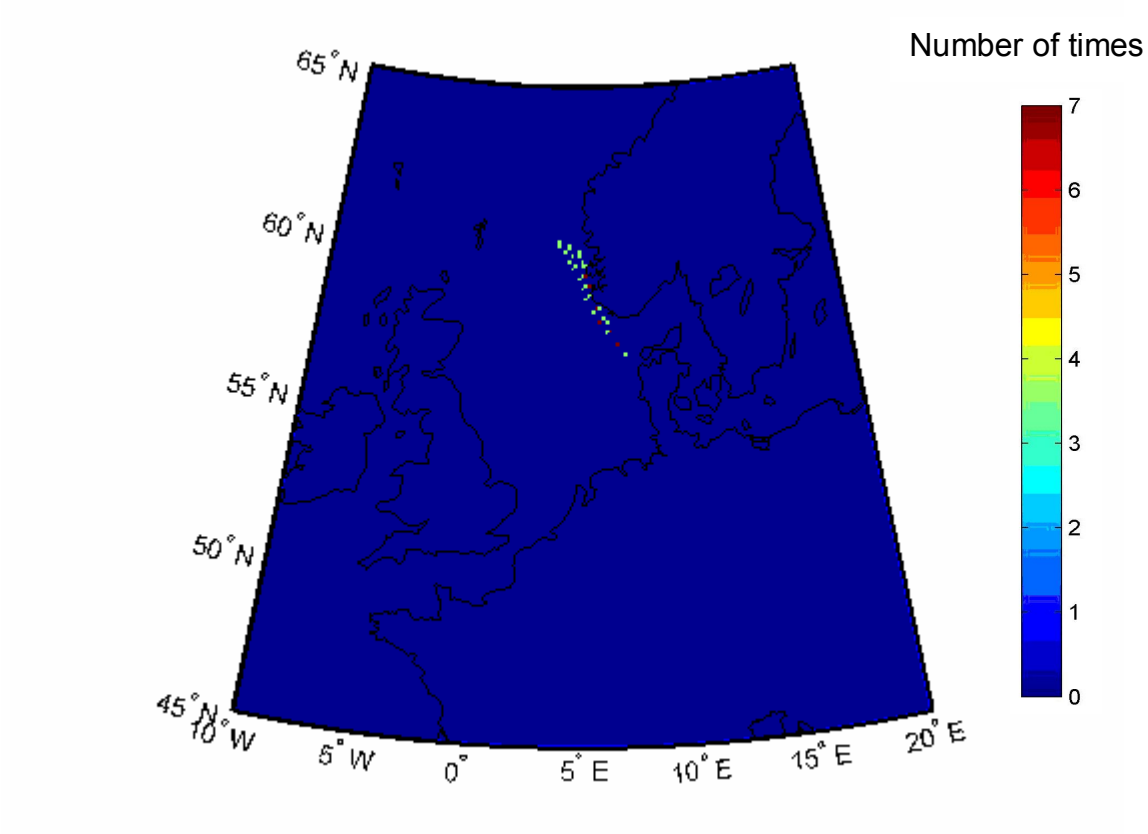

Figure 14. Map of the number of times that there is new particle formation of 1.5 nm diameter particles registered at the Høvsøre site during 31 March 2012. The resolution of the grid cells is 0.1 degree for the latitude and 0.2 degree for the longitude.

7. Results

7.1. Analysis of size distributions

In the given study, size distributions obtained from the SMPS system and AIS that operated at Høvsøre from March 9 2012 till May 31 2012 were analyzed. The SMPS analysis showed that the total number concentration for particles in the size range 12 to 500 nm diameter in March was higher than in April and May (Figure 15) and was 2666 cm^{-3} on average. In April and May the concentration is on average 1330 cm^{-3}. The days when NPF were detected are characterized by an increase of the total particle number concentration after the start of the formation as shown in Figure 16 for March 31, 2012. Figure 15 also shows however, that during days prior to an event and the days after the event, there concentration could be higher. In other words, the formation events are not always giving a very high increase in the particle number concentration, and during a few of the events in April and May, new particle formation is giving a concentration increase below the average total number concentration in March.

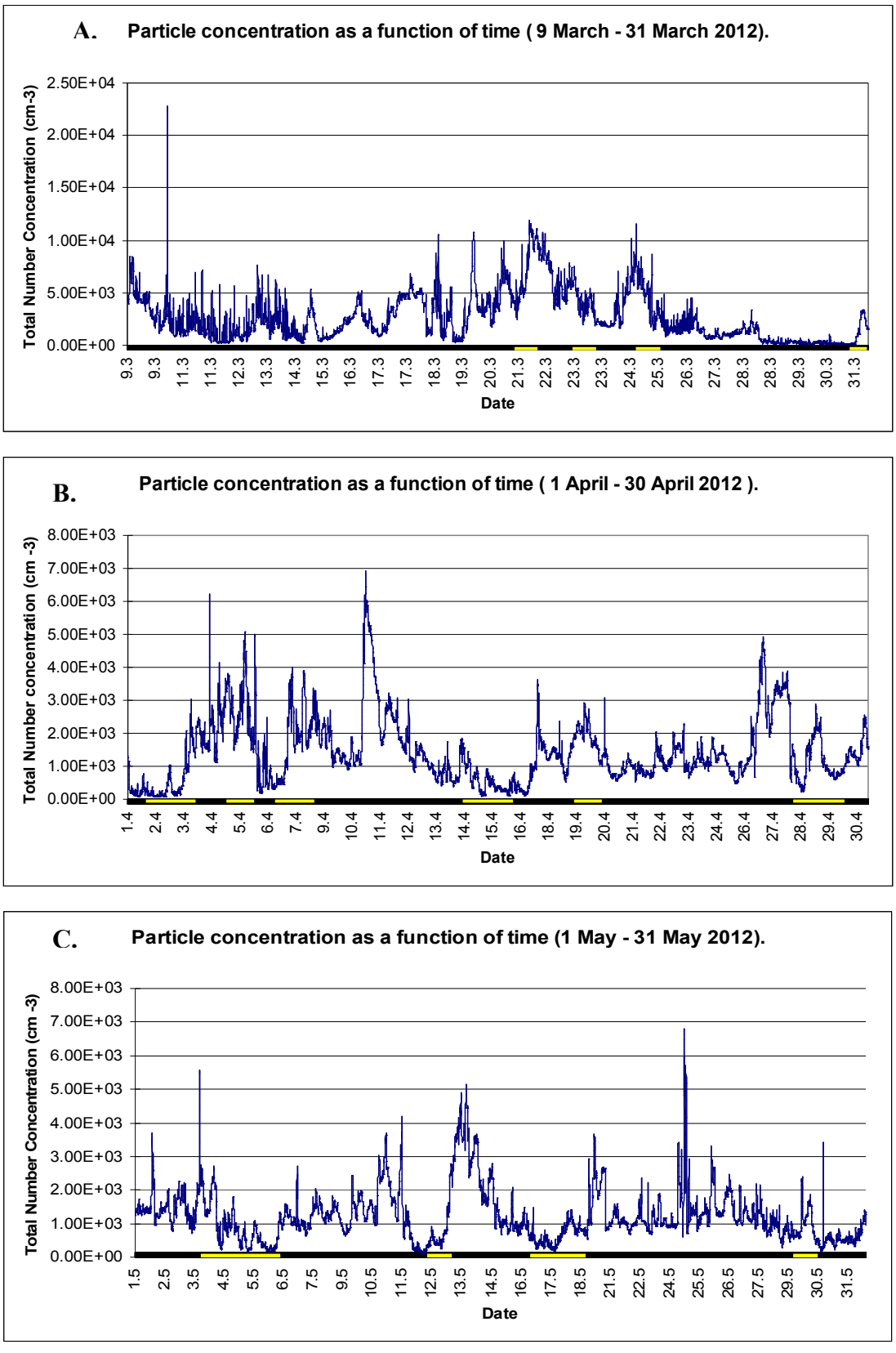

*Figure 15. Total number concentration of particles between 12 nm and 500 nm diameter at Høvsøre from SMPS data measured: **A**.: 9 March-31 March 2012, **B**.: 1April – 30 April 2012, **C**. 1 May – 31 May 2012. Yellow lines depict days when NPF events were detected.*

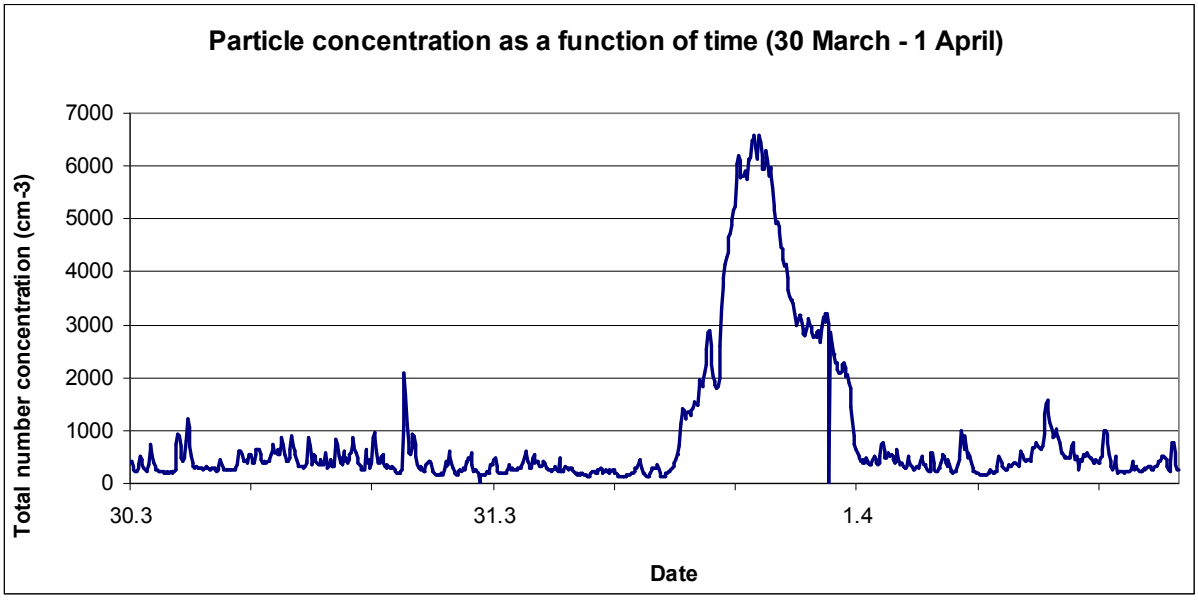

Figure 16.Total number concentration calculated from the SMPS data during three days, before an event day (March 30), during an event day (March 31), and after an event day (Apri1 1).

The median size distribution from the entire measurement period shows that particles from the Nucleation and Aitken modes dominate the number concentration (Figure 17). Also particles in the accumulation mode are present at Høvsøre. Since large particles representing the coarse mode were not measured in this project, these particles are not observed in the size distribution. The 25 and 75 percentiles show that the variability in the nucleation and Aitken modes are larger than in the accumulation mode, meaning that long range transport of aged particles in the accumulation mode was relatively stable during the measurement period. Particles in the Aitken mode also come from long distance transported particles as well as from sea spray emissions and ship emissions. The study by Kivekäs et al. (2014) for example, shows that about 10 % of all particles in the Aitken mode come from ship emissions at Høvsøre during the entire year 2012.

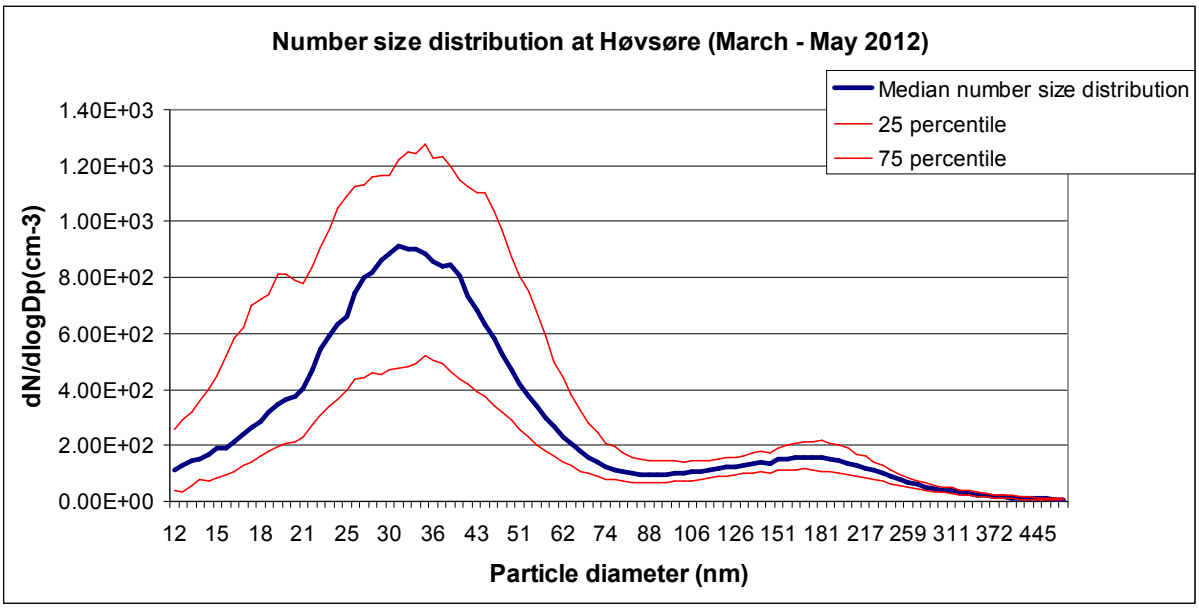

Figure 17. Median number size distribution, 25 and 75 percentile of number concentrations measured on 9 March -31 May 2012 at Høvsøre.

The size distribution from the SMPS covers the size range between 12 and 500 nm diameter, whereas the AIS size distribution covers the range between 1 and 40 nm diameter. Thus, the size distributions obtained from the SMPS and from the AIS were combined to get the number size distribution for particles 1-500 nm. The combined size distribution makes it possible to detect formation of small particles with diameters around 1.5 nm. During periods when both instruments overlapped, only the part with the AIS data between 1 and 12 nm diameter was used for the analysis.

During an NPF event, the size distribution displays an increase of the particle concentration at the nucleation mode, and then the particles grow by condensation for several hours. If particles are formed over a larger area, the growth of particles can be followed for many hours or even several days at one measurement station. These events can be terminated by local pollution or by a sudden change of air mass (Hussein, et al. 2009). The size distributions can also exhibit an increase of the concentration of very small particles (2-25 nm) but without further growth, or with a very weak growth. These events are not regionally extensive.

Analysis of aerosol particle size distribution gained from several measurement stations in 2008-2009 including Birkenes and Cabauw showed that background number concentrations of aerosol particles in Cabauw are much higher than in Birkenes (Asmi, at al. 2011). The median total aerosol particle concentration with diameter between 30 nm and 500 nm in Birkenes is 667 cm^{-3} and in Cabauw it is 5301 cm^{-3} (Table 4). Cabauw is surrounded by several large cities at a distance of about 20 to 40 km from the station, for example Amsterdam, Hague, Utrecht, Dordrecht, and Hertogenbosch, why it is much more polluted than the other stations in this study.

Table 4. Summary from the total particle concentration with diameters between 30-500 nm from Birkenes (2008- 2009), Cabauw (2008 - 2009) and Høvsøre (spring 2012).

	Median values of total particle concentration in the Aitken and Accumulation modes (cm^{-3})
Birkenes (2008-2009)	667
Cabauw (2008-2009)	5301
Høvsøre (spring 2012)	1010

The median number size distribution obtained at the Birkenes site during 2010 showed that two modes can be distinguished during the spring season: one Aitken mode and one accumulation mode (Figure 18).

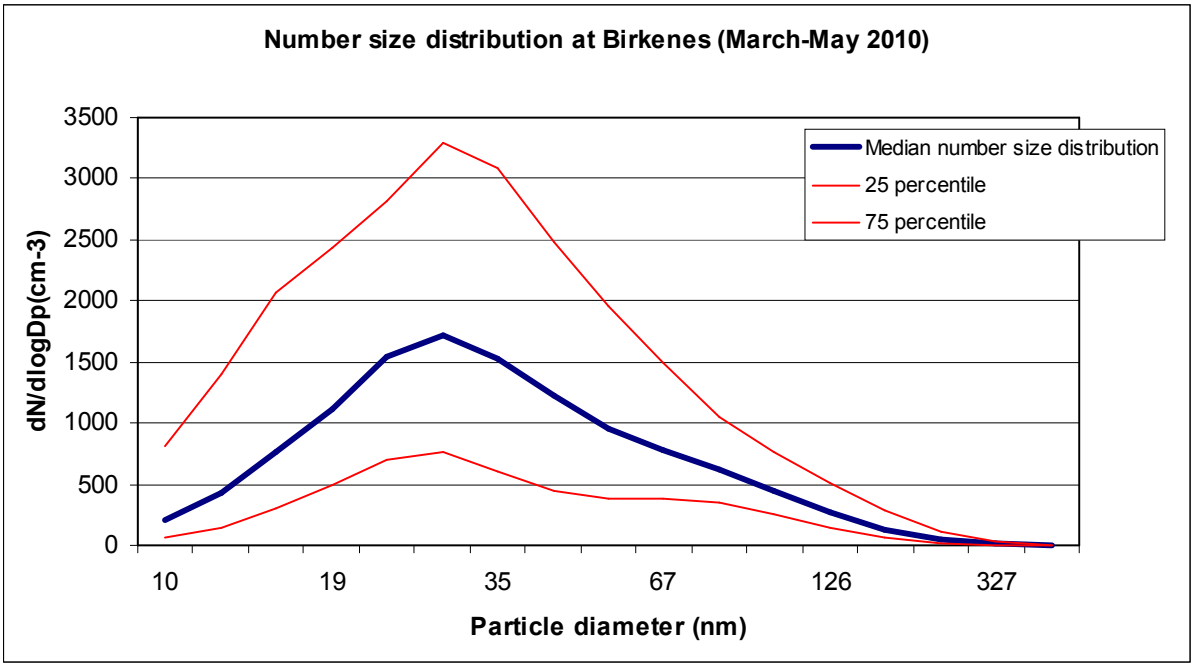

Figure 18. Median number size distribution, 25 and 75 percentile of number concentrations measured on March -May 2010 at Birkenes.

In Cabauw, the number size distributions show 1 clear Aitken mode during the spring season, and a relatively weaker accumulation mode (Figure 19). The total particle number concentration in the accumulation mode is also high at Cabauw, however relatively much lower than the Aitken mode due to the proximity to the larger cities.

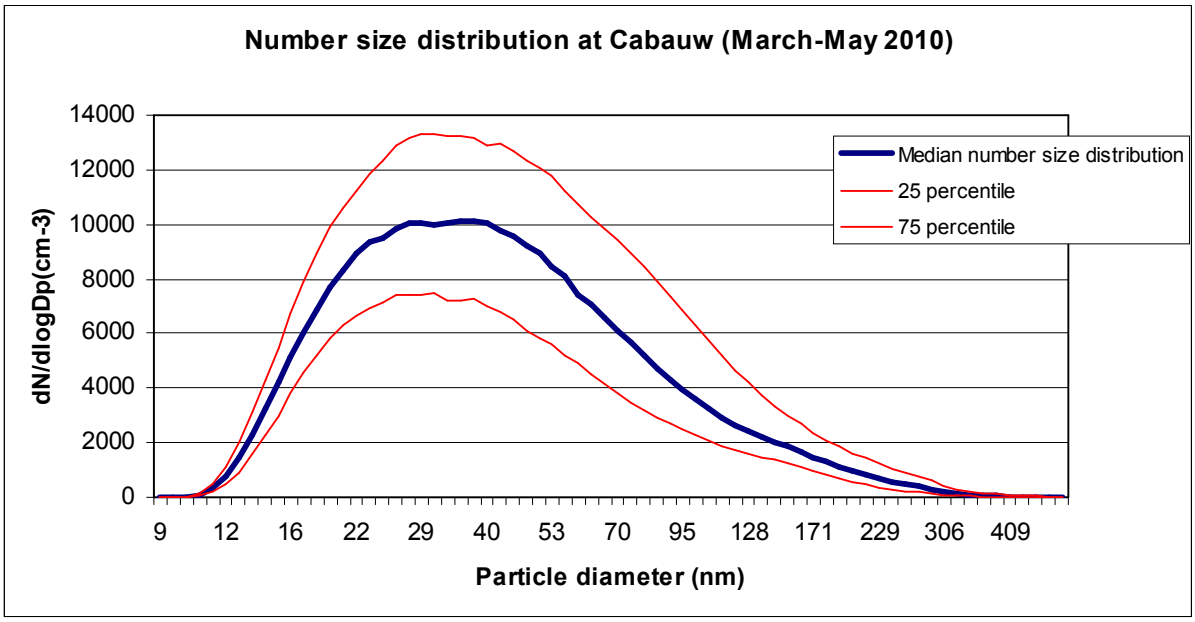

Figure19. Median number size distribution, 25 and 75 percentile of number concentrations measured on March -May 2010 at Cabauw

7.2. Statistics of new particle formation events

NPF were observed at Birkenes, Cabauw and Høvsøre, but the probability to observe events varies from site to site. Size distributions obtained from the 3 studied sites were analyzed and all the measured days were distributed according to the classification described earlier in chapter 5.1 into class I event days, class II event days, undefined and non-event (Table 5). Days with bad or missing data were excluded from the statistics.

Table 5. Number of days with classification of event data at Birkenes, Cabauw and Høvsøre. The percentage of days with specific classification is shown in brackets.

Study site	Dates	Days of measurement	Class I event	Class II event	Undefined	Non-event
Birkenes	07.10.2009-06.23.2010	318	13(4%)	24(7%)	158(50%)	123(39%)
Cabauw	01.01.2010-12.26.2011	509	52(10%)	14(3%)	237(47%)	206(40%)
Høvsøre	03.09.2012-05.31.2012	78	21(27%)	20(26%)	21(27%)	16(20%)

New particle formation events were detected at the Danish Høvsøre site during March, 9 – May 31 2012 by the SMPS and AIS instruments. All the nucleation bursts started in the morning between 7 and 12 o'clock. After classification of the events it was established that almost 3 months of data showed 21 days with nucleation events of type I that accounts for 27% of all period of measurements excluding days with bad or no data (Figure 20.). The class I event frequency varied between 15 % in March and 34 % in April at Høvsøre. The lower frequency of class I events in March might be a consequence of the higher background concentration, see Figure 9. A higher concentration of background particles will decrease the probability to observe an event, since the already existing background particles will create a relatively large coagulation sink of the newly formed particles during new particle formation events (Kristensson et al., 2008). They are also acting as a sink for the condensing vapors that could potentially take part in the new particle formation (Kristensson et al., 2008).

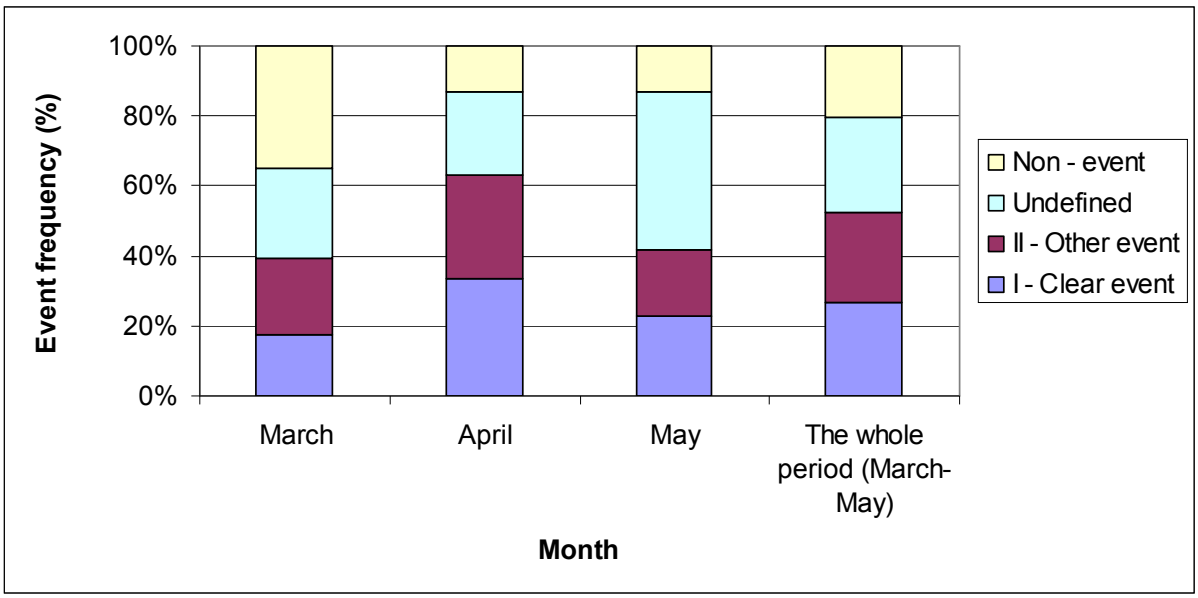

Figure 20. Frequency of new particle formation events as a function of month at the Høvsøre site during March, 9 – May, 31 2012. Days with bad data were excluded from the statistics.

Please note that the amount of days classified as type I events using only the SMPS data was 9 days less than for data where the classification is based on both the SMPS and AIS. It means that due to limits of the SMPS, which can not detect particles below 12 nm in diameter, some NPF events were not discovered.

7.3 NanoMap results for Høvsøre

Using the NanoMap methodology described in chapter 5, or by Kristensson et al. (2014), the formation of 1.5 nm diameter particle as function of geographical position was calculated, and presented in Figure 21. In addition to this, a map of the number of events as function of geographical grid cells was also created (Figure 22). A considerable part of the nanoparticles during the events were formed over the North Sea, but occasionally, the particles were also formed over the Danish continent.

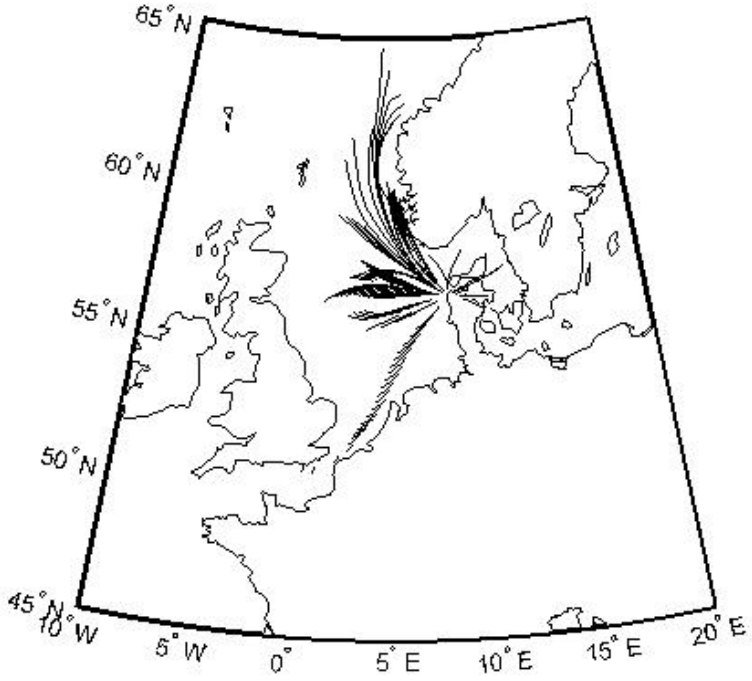

Figure 21. Map of formation of 1.5 nm diameter particles according to the NanoMap method calculated at the Danish Høvsøre site during March, 9 – May, 31 2012.

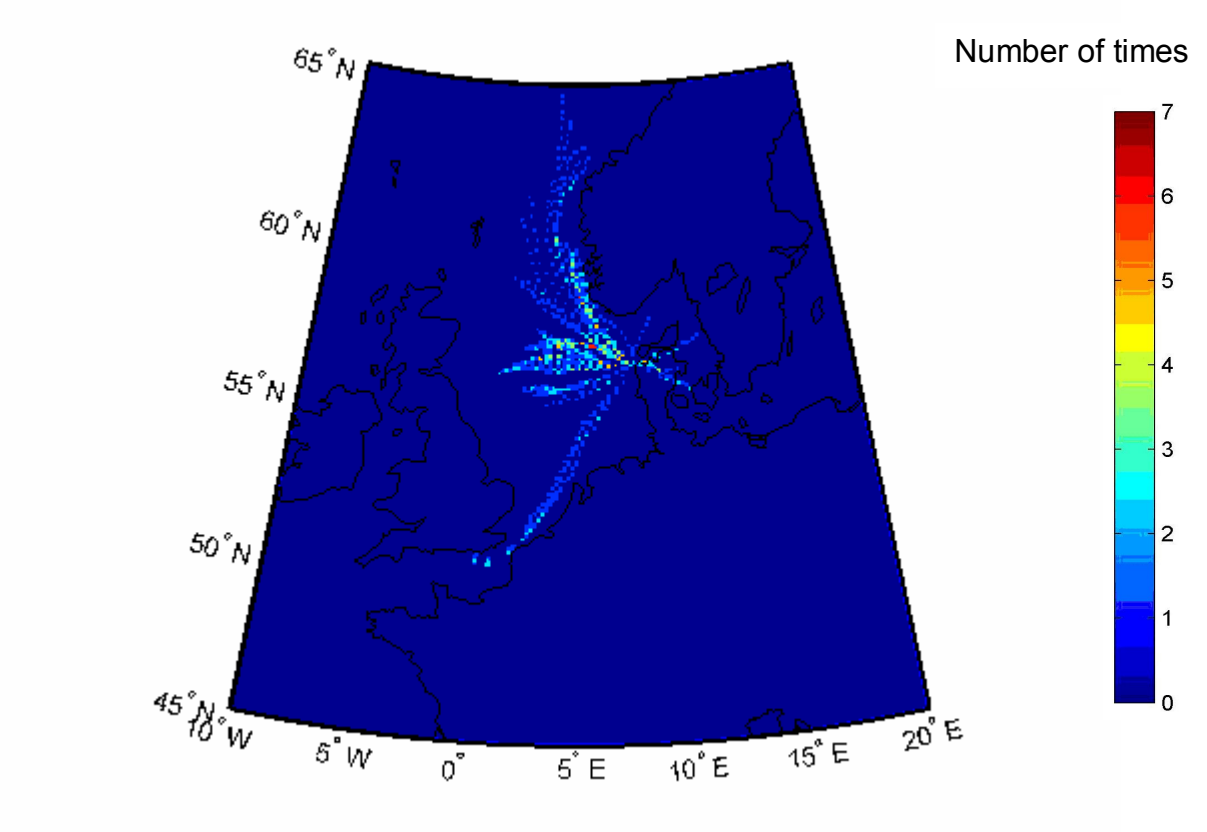

Figure 22. Map of the number of times that there is new particle formation of 1.5 nm diameter particles according to the NanoMap method for Høvsøre during March, 9 – May, 31 2012.

7.4 NanoMap results for Birkenes and Cabauw

Less days were registered as event days at Birkenes and Cabauw compared to Høvsøre (see Table 5) since many NPF events were missed due to lack of information about particle number concentrations below 10 nm diameter. More than 80% of the days were classified as Non-events or Undefined events at Birkenes. In Cabauw, the number of Non-events or Undefined was smaller and makes up around 60%. Nevertheless, there are some events over the North Sea, but the majority of NPF events were over land for both Birkenes and Cabauw (Figure 23). There were 4% and 10 % class I events out of all measured days excluding days with bad data at Birkenes and Cabuaw respectively.

A. Birkenes 2009-2010

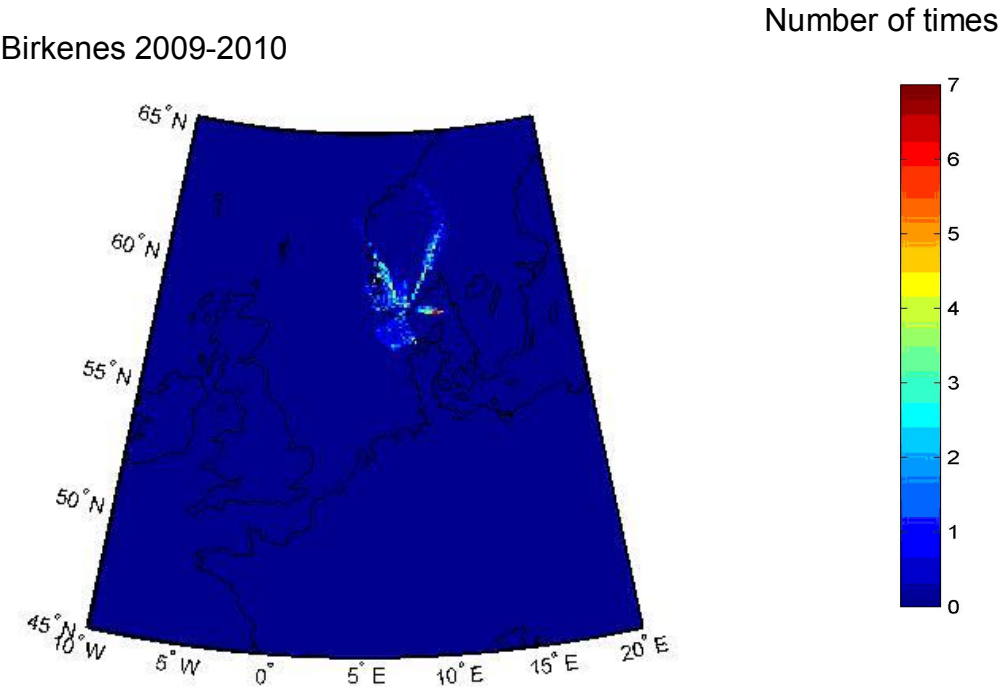

B. Cabauw 2010-2011

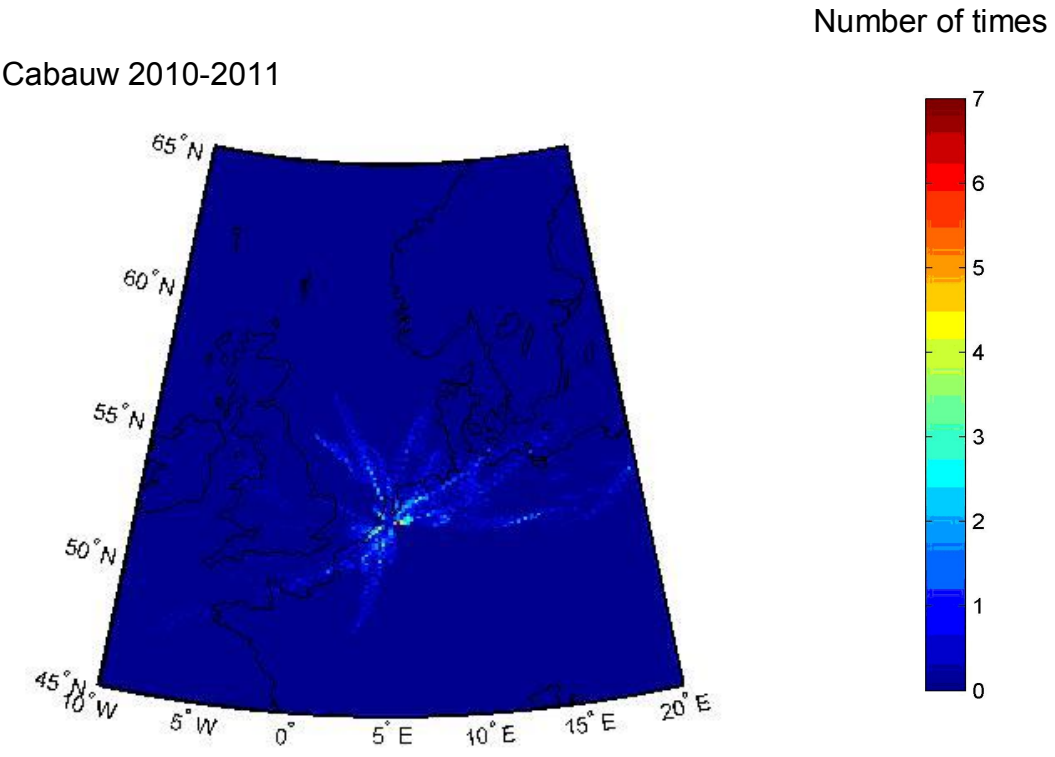

Figure 23. Map of the number of times that there are new particle formation events with particle formation at 1.5 nm diameter at Birkenes during July, 7 2009 – June, 23 2010 (A) and Cabauw during January, 1 2009 – December 26 2011 (B).

8. Discussion

At all three study sites, Birkenes, Cabauw, and Høvsøre, NPF events were detected over the North Sea where main shipping lanes are located. The largest port in Europe is located in Rotterdam, and there is a huge harbor in Hamburg. Taking into account that shipping is the main contributor to SO_2 emissions in marine atmospheres, it is possible to assume that the proximity of ship lanes can be one of the sources of NPF in the North Sea (Figure 24). Beside SO_2, ships emit such components as NO_x, volatile organic carbon (VOC) pollutants, which can also affect the aerosol particle concentration in the atmosphere.

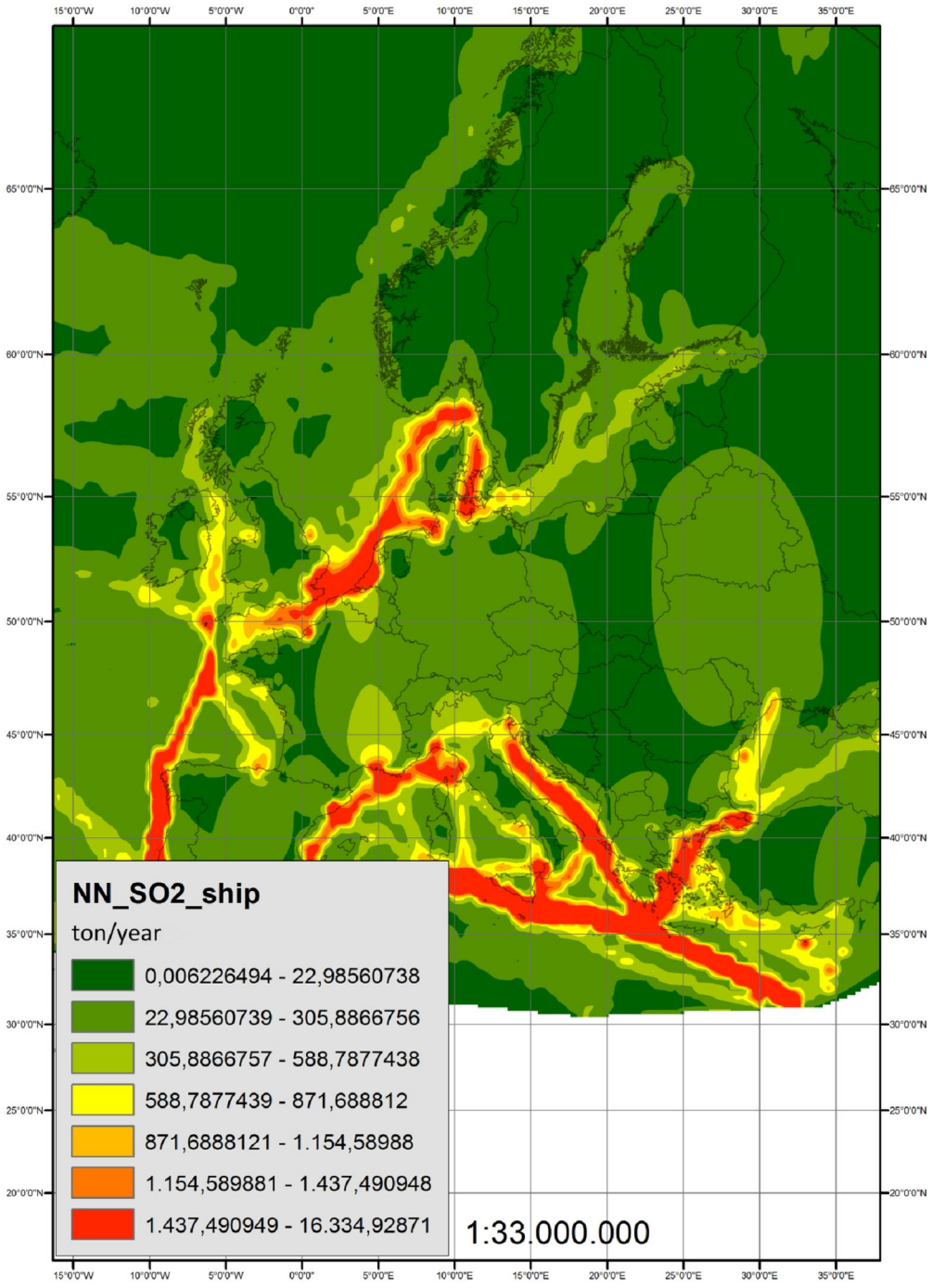

Figure 24. Shipping SO_2 emissions 2010 according to Lange (2013).

Analyzing all the data about the geographical location of the registered NPF events and the map of shipping SO_2 emissions it is possible to see that many aerosol particles were formed along the shipping routes at the North Sea. It can be assumed that emissions from vessels can play a role in NPF at the coastal sites.

Probably formation of aerosol particles at Høvsøre can be induced by emissions of VOC compounds working as precursors for NPF due to oil flaring from oil stations situated at the North Sea on the background of relatively clean air masses coming from the North-North-West.

Another potential source of aerosol particles during NPF events is biogenic emissions from the forest or the ocean. Biogenic volatile organic compound (BVOC) emissions in the marine environment can occur during algae blooming. Algae is a phytoplankton species that can be found at upper layers of the sea where there is enough light for photosynthesis. Marine phytoplankton is a source of organic sulfate since it produces dimethyl sulfide (DMS) which oxidizes to sulphur dioxide in the atmosphere (Charlson et al., 1987). As was mentioned above, sulphuric acid is produced from sulphur dioxide and is a main component in the nucleation process.

In addition to DMS emissions, algae might change the density of the surface water making it thicker and thus affect natural sea spray production. If less sea spray is produced, there are less large aerosol particles in the atmosphere to coagulate with the smaller particles produced during NPF events. So, algae may have a positive feedback on the NPF due to the sea spray influence.

It is difficult to predict periods of algae blooming. Usually their period of blooming starts at the middle of the February with maximum in March, so spring is a period when DMS concentrations can increase considerably. That is why it is important to understand if there were algae blooming around Høvsøre when nucleation events were observed. Since algae contain chlorophyll where photosynthesis occurs, monitoring of chlorophyll concentrations allows identifying the distribution of algae blooms (Figure 25). During the measurement campaign in Høvsøre algae blooming was strong in March, then it decreased in April and May. (http://www.waqss.de/about.html) Analysis of the maps of chlorophyll concentrations showed that NPF events were observed both during the days when high levels of algae is detected and during the days with low amount of algae. Thus, there is no clear evidence about correlation of algae blooms and NPF events detected at Høvsøre. This does not dismiss the role of algae emissions for NPF events. Maybe the periods with low emissions are also producing enough DMS for NPF.

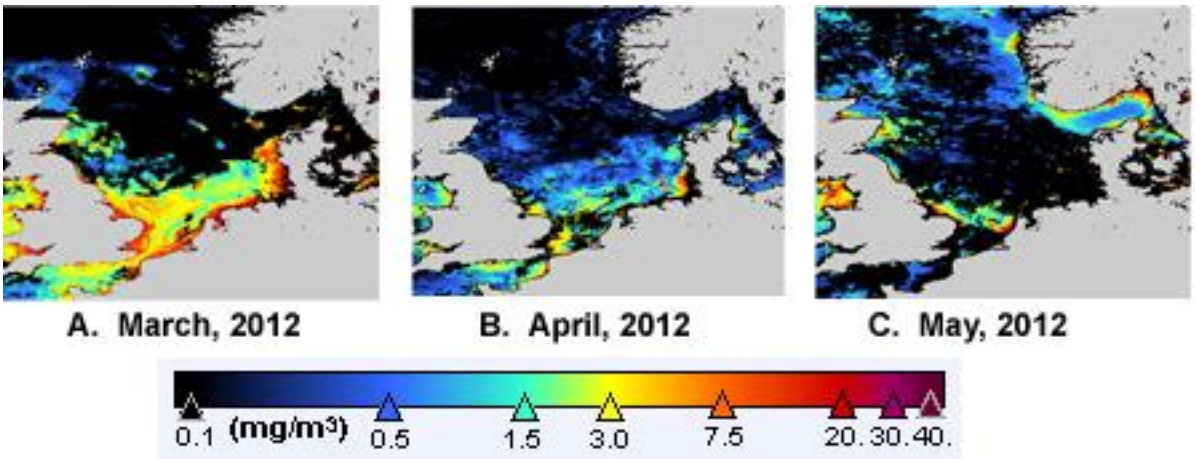

Figure 25. Chlorophyll concentrations for the North Sea for the days when NPF events class I were observed at Høvsøre. A. March, 31 2012, B. April, 16 2012, C. May, 6 2012. Data from the MODIS sensor of the Aqua satellite (WAQSS 2014).

Another possible source of the sulphuric acid and organic compounds needed for NPF is the emissions from continental biogenic VOC sources and anthropogenic activities in Great Britain and Norway.

Several possible sources of aerosol particles were discussed here, but it is impossible to identify the dominating source of aerosol particles from NPF registered at Høvsøre. Probably, a mixture of shipping emissions, continental pollutants, oil flaring, and biogenic VOC emissions from the sea surface or forest favor new particle formation events.

Analysis of wind directions during NPF events at Høvsøre demonstrated that westerly winds dominated (Figure 26) on the days when nucleation events were detected. Very clear “banana”-shaped events were observed at low relative humidity and when the wind rapidly changed its direction. On the other hand, when winds came from more polluted regions, less NPF events occurred. Pollutants from industrial zones suppress formation of new aerosol particles since gas molecules condense on pre-existing particles rather then form new aerosol particles, and since coagulation scavenge newly formed particles in the nucleation mode.

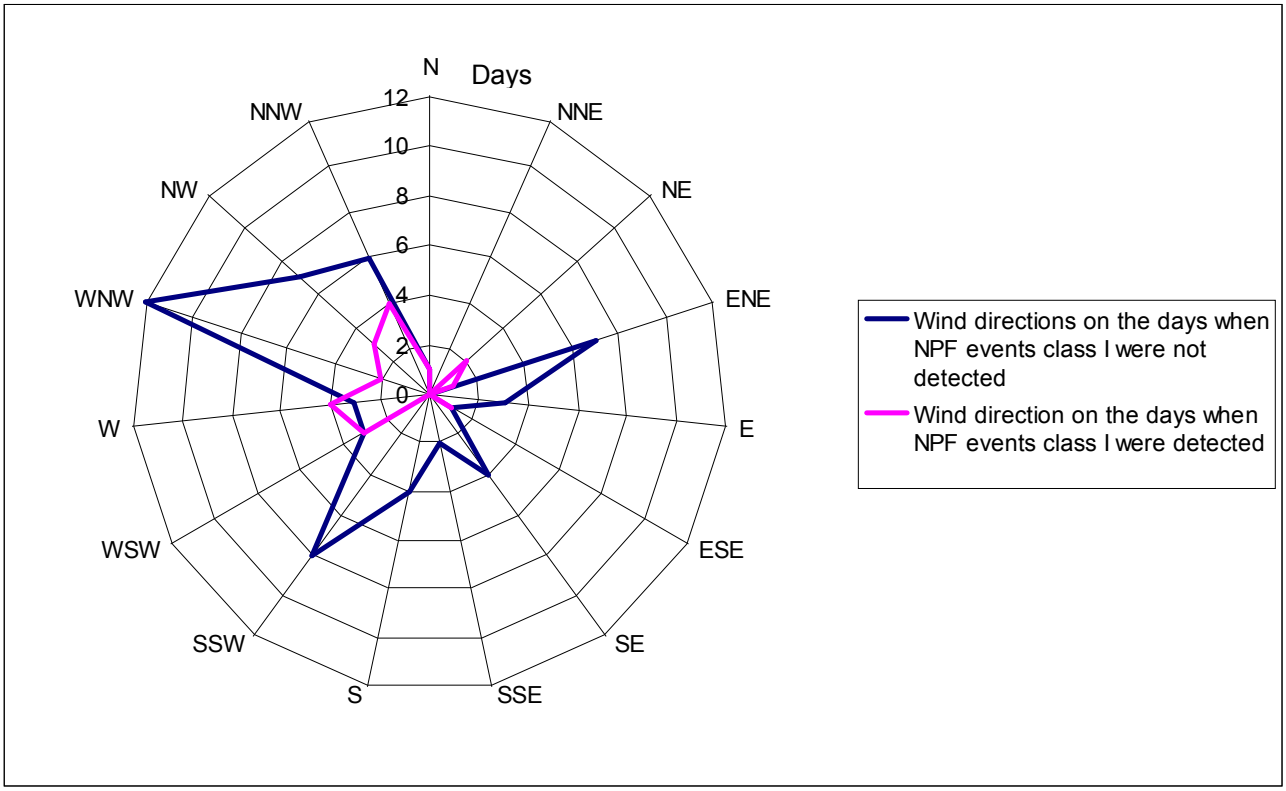

Figure 26. Wind Rose during measuring campaign at Høvsøre March, 9 2012 – May, 31 2012. Wind directions on the days when NPF events class I were detected are depicted in blue and wind directions during the days when NPF were detected are depicted in pink.

The majority of the class I events were observed under cyclonic conditions when air moves anti-clockwise around a low pressure region in the center (Lange, 2013). These low pressure systems brought clean air masses from the Arctic Sea and the North Sea with low background concentrations of aerosol particles. This condition favor to NPF since there is less surface area where vapors can condense on. However, a few events were also detected under anti-cyclonic conditions (high pressure in the center of the system) when the air came from polluted regions (Lange, 2013), especially to the west or south of Høvsøre.

It is very likely that some chemical compounds favorable for nucleation events came with pollution and triggered the nucleation of new particles. It is unclear what compounds they are, but from more southerly air masses there is a higher probability of a stronger contribution from anthropogenic and biogenic continental emissions.

9. Conclusions.

To investigate whether NPF events are observed at the marine boundary layer of the North Sea measurements of aerosol particle size distributions were organized at the Danish Høvsøre site during March, 9 – May, 31 2012.The size distribution was measured by two instruments: AIS (for charged particles 2 – 40 nm diameter) and SMPS (for particles 12-500 nm diameter). In addition to data from Høvsøre, size distributions from Norwegian Birkenes (2009-2010) and Dutch Cabauw (2010-2011) obtained from DMPS and SMPS instruments were analyzed as well.

Analysis of almost 3 months of data measured at Høvsøre showed that nucleation events happened over the North Sea quite often. 27% of all measured days were classified as class I event days. The majority of class I events in Høvsøre happened when clean air masses came from the Arctic Sea and Atlantic Ocean under cyclonic meteorological conditions. This can be explained by a concentration decrease of the preexisting particles, which are not favoring the nucleation process.

Since particles below 10 nm diameters were not measured at Birkenes and Cabauw, many NPF events were not registered. Clear events were detected only at 4% days at Birkenes and around 10% at Cabauw. At these two sites nucleation took place mostly over the land surface.

Using the NanoMap method, maps of where 1.5 nm aerosol particles are formed close to Høvsøre, Cabauw and Birkenes were constructed. The method utilizes back trajectory data about origin of air masses and parameters of formation events defined from visual inspection of size distribution plots.

The majority of the detected nucleation events at Høvsøre occurred over the sea, near the shipping lanes and can be caused by SO_2 emissions from the vessels, algae blooming or emissions from oil platforms at the North Sea. Also continental emissions might have contributed. Hence, a combination of different emission sources could have influenced the NPF. Due to the influence of many sources at the same time, it was hard to conclude which of these sources were most important for the NPF. Modeling might shed more light in this issue. Another possibility is to perform measurements at a specific place where only one or two sources could possibly contribute to the NPF events.

References

Aerosols, Clouds, and Trace gases Research InfraStructure Network, 2013. URL http://www.actris.net (last accessed 2014-03-03)

Air Resources Laboratory, 2012. URL http://www.arl.noaa.gov/ready/hysplit4.html. (last accessed 2014-03-03)

Andreae, M. O., 2007. Aerosols before pollution, Science, 315, 50–51.

Asmi, A., Wiedensohler, A., Laj, P., Fjaeraa, A.-M., Sellegri, K.,Birmili, W., Weingartner, E., Baltensperger, U., Zdimal, V., Zikova, N., Putaud, J.-P., Marinoni, A., Tunved, P., Hansson, H.-C., Fiebig, M., Kivekäs, N., Lihavainen, H., Asmi, E., Ulevicius, V., Aalto, P.P., Swietlicki, E., Kristensson, A., Mihalopoulos, N., Kalivitis, N., Kalapov, I., Kiss, G., de Leeuw, G., Henzing, B., Harrison, R.M., Beddows, D., O'Dowd, C., Jennings, S.G., Flentje, H., Weinhold, K., Meinhardt, F., Ries, L., Kulmala, M. 2011. Number size distributions and seasonality of submicron particles in Europe 2008–2009. Atmos. Chem. Phys., 11, 5505-5538.

Charlson, R. J., Lovelock, J. E., Andreae, M. O. and Warren, S. G. (1987). "Oceanic phytoplankton, atmospheric sulphur, cloud albedo and climate". Nature 326 (6114): 655–661.

Crumeyrolle, S., Manninen, H. E., Sellegri, K., Roberts, G., Gomes,L., Kulmala, M., Weigel, R., Laj, P., and Schwarzenboeck, A. 2010. New particle formation events measured on board the ATR-42aircraft during the EUCAARI campaign, Atmos. Chem. Phys.,10, 6721–6735,doi:10.5194/acp-10-6721-2010.

Curtius, J., 2009, Nucleation of atmospheric particles, The European Physical Journal Conferences 1, 199-209.

Dal Maso, M., Kulmala, M., Riipinen, I., Wagner, R., Hussein, T., Aalto, P.P., and Lehtinen, K.E.J., 2005. Formation and growth of fresh atmospheric aerososls: eight years of aerosol size distribution data from SMEAR II, Hytiälä, Finland, Boreal Environ. Res., 10, 323-336.

Draxler, R. R. and Hess, G. D. 1997. Description of the Hysplit 4 modelling system. NOAA Tech Memo, ERL, ARL-224, NOAA Air Resources Laboratory, Silver Spring, MD, 24 pp.

Gunturu, U. B., 2010. Aerosol-Cloud Interactions: A New Perspective in Precipitation Enhancement Ph.D. Thesis, Department of Earth, Atmospheric and Planetary Sciences, MIT, 186 pp.

Haywood, J., and Boucher, O. 2000. Estimates of the direct and indirect radiative forcing due to tropospheric aerosols: A review. *Rev. Geophys.,* 38(4), 513–543, doi:10.1029/1999RG000078.

Heinzerling, D., Hysplit trajectory modeling and clustering techniques: computation, error analysis, and applcations, 2005. Master Thesis, The University of Texas at Austin.

Hinds, W. C., 1999. Aerosol technology: properties, behavior, and measurement of airborne particles 2nd edition. New York, USA: John Wiley. ISBN 978-0-471-19410-1.

Holmes, N.S. 2007. A review of particle formation events and growth in the atmosphere in the various environments and discussion of mechanistic implications. Atmospheric Environment 41, 2183-2201.

Hussein, T., Junninen, H., Tunved, P., Kristensson, A., Dal Maso, M., Riipinen, I., Aalto, P. P., Hansson, H.-C., Swietlicki, E., and Kulmala, M., 2009. Time span and spatial scale of regional new particle formation events over Finland and Southern Sweden, Atmos. Chem. Phys., 9, 4699-4716, doi:10.5194/acp-9-4699-2009.

Hyvärinen, A.-P., Komppula, M., Engler, C., Kivekäs, N., Kerminen, V.-M., Dal Maso, M., Viisanen, Y., and Lihavainen, H.. 2008. Atmospheric new particle formation at Utö, Baltic Sea 2003–2005, Tellus B, 60, 345–352.

IPCC, 2013: Climate Change 2013: The Physical Science Basis. Contribution of Working Group I to the Fifth Assessment Report of the Intergovernmental Panel on Climate Change. Stocker, T. F., D. Qin, G.-K. Plattner, M. Tignor, S. K. Allen, J. Boschung, A. Nauels, Y. Xia, V. Bex and P. M. Midgley (eds.) Cambridge University Press, Cambridge, United Kingdom and New York, NY, USA

Janhäll, S., Andreae, M. O., Pöschl, U., 2010. Biomass burning aerosol emissions from vegetation fires: particle, number and mass emission factors and size distributions, Atmos. Chem. Phys., 10, 1427–1439.

Kivekäs, N., Massling, A., Grythe H., Lange R., Rusnak V., Carreno S., Skov, H., Swietlicki, E., Nguyen, Q., T., Glasius M., and Kristensson, A. Contribution of ship traffic to aerosol particle concentrations downwind of a major shipping lane. Submitted to Atmospheric Chemistry and Physics Discussion 2014.

Kristensson, A., 2005. Aerosol Particle Sources Affecting the Swedish Air Quality at Urban and Rural Level. Academic dissertation, Division of Nuclear Physics, Department of Physics, Lund University, Lund, Sweden. ISBN 91-628-6573-0.

Kristensson, A., Dal Maso, M., Swietlicki, E., Hussein, T., Zhou, J., Kerminen, V.-M., and Kulmala, M., 2008. Characterization of new particle formation events at a background site in Southern Sweden: relation to air mass history. *Tellus*, 60B, 330–344.

Kristensson, A., 2013. A compendium in atmospheric aerosol particles for the atmospheric chemistry course. Lund University, Sweden.

Kristensson, A., Johansson, M., Swietlicki, E., Kivekäs, E., Hussein, T., Nieminen, T., Junninen, H., Tunved, P., Kulmala, M., and Dal Maso, M., 2014. NanoMap: Geographical mapping of atmospheric new particle formation through analysis of particle number size distribution and trajectory data. Submitted to Boreal Environment Research 2014.

Kulmala, M., Pirjola, L. and Mäkelä, J.M. 2000. Stable sulphate clusters as a source of new atmospheric particles. Nature, 404, 66-69.

Kulmala, M., Suni, T., Lehtinen, K. E. J., Dal Maso, M., Boy, M., Reissell, A., Rannik, Ü., Aalto, P., Keronen, P., Hakola, H., Bäck, J., Hoffmann, T., Vesala, T., and Hari, P., 2004. A new feedback mechanism linking forests, aerosols, and climate, Atmos. Chem. Phys., 4, 557-562, doi:10.5194/acp-4-557-2004.

Kulmala, M., Kontkanen, J., Junninen, H., Lehtipalo, K., Manninen, H.E., Nieminen, T., Petäjä, T., Sipilä, M., Schobesberger, S., Rantala, P., Franchin, A., Jokinen, T., Järvinen, E., Äijälä, M., Kangasluoma, J., Hakala, J., Aalto, P.P., Paasonen, P.,

Mikkilä, J., Vanhanen, J., Aalto, J., Hakola, H., Makkonen, U., Ruuskanen, T., Mauldin, R.L. 3rd, Duplissy J., Vehkamäki, H., Bäck, J., Kortelainen, A., Riipinen, I., Kurtén, T., Johnston, M.V., Smith, J.N., Ehn, M., Mentel, T.F., Lehtinen, K.E., Laaksonen, A., Kerminen, V.-M. & Worsnop, D.R. 2013. Direct observations of atmospheric aerosol nucleation. Science 339: 943–946.

Köhler, H., 1936. The nucleus in and the growth of hygroscopic droplets. Transactions of the Faraday Society 32 (1152-1161).

Lange, R., NanoShip: Investigation of shipping induced new particle formation at the North Sea, 2013. Master Thesis, Department of Chemistry, Aarhus University, Denmark.

Mather TA, Pyle DM, Oppenheimer C. Tropospheric volcanic aerosol. In: Robock A, Oppenheimer C, eds. Volcanism and the Earth's Atmosphere. Washington, DC: AGU; 2003, 165–176.

Mirme, A., Tamm, E., Mordas, G., Vana, M., Uin, J., Mirme, S., Bernotas, T., Laakso, L., Hirsikko, A., and Kulmala, M., 2007. A wide-range multi-channel Air Ion Spectrometer, Boreal Env. Res., 12, 247–264.

Merikanto, J., Spracklen, D. V., Mann, G. W., Pickering, S. J., and Carslaw, K. S., 2009: Impact of nucleation on global CCN, Atmos. Chem. Phys., 9, 8601-8616, doi:10.5194/acp-9-8601-2009.

Pope, C. A., III, and Dockery, D. W., 2006. Health Effects of Fine Particulate Air Pollution: Lines that Connect. *J. Air & Waste Manage. Assoc.*, 56. 709–742.

Quant FR, R Caldow, GJ Sem, and TJ Addison, 1992. Performance of Condensation Particle Counters with Three Continuous-Flow Designs, J. Aerosol Sci. 23:S405-S408. (TSI paper A79)

Seinfeld J. H. and Pandis S. N., 2006 Atmospheric Chemistry and Physics: From Air Pollution to Climate Change, 2nd edition, J. Wiley, New York.

Sipilä, M., Berndt, T., Petäjä, T., Brus, D., Vanhanen, J., Stratmann, F., Patokoski, J., Mauldin, R. L., Hyvärinen, A.P., Lihavainen, H., and Kulmala, M., 2010. The Role of Sulfuric Acid in Atmospheric Nucleation, Science, 327, 1243 1246, doi:10.1126/science.1180315.

Stohl A., Computation, accuracy and applications of trajectories—A review and bibliography, Atmospheric Environment, Volume 32, Issue 6, 1 March 1998, Pages 947-966.

TSI Incorporated, 2002. Model 3010 Condensation Particle Counter Instruction Manual.

Wang, S.C. and R.C. Flagan, 1990. Scanning electrical mobility spectrometer. *Aerosol Science and Technology*, 13(2): 230-240.

WAQQS, Water Quality Service System, 2014. MODIS chlorophyll data from the Aqua satellite. http://www.waqss.de/archive.html (last accessed: 2014-03-03).

Weber, R. J., Moore, K., Kapustin, V., Clarke, A., Mauldin, R. L., Kosciuch, E., Cantrell, C., Eisele, F., Anderson, B., and Thornhill, L., 2001 Nucleation in equatorial Pacific during PEM-Tropics B: Enhanced boundary layer H_2SO_4 with no particle production. *J. Geoph. Res.*, 106 (23), 32,767-32,776.

Seminar Series

Institutionen för naturgeografi och ekosystemvetenskap, Lunds Universitet.

Student examensarbete (Seminarieuppsatser). Uppsatserna finns tillgängliga på institutionens geobibliotek, Sölvegatan 12, 223 62 LUND. Serien startade 1985. Hela listan och själva uppsatserna är även tillgängliga på LUP student papers (www.nateko.lu.se/masterthesis) och via Geobiblioteket (www.geobib.lu.se)

The student thesis reports are available at the Geo-Library, Department of Physical Geography and Ecosystem Science, University of Lund, Sölvegatan 12, S-223 62 Lund, Sweden. Report series started 1985. The complete list and electronic versions are also electronic available at the LUP student papers (www.nateko.lu.se/masterthesis) and through the Geo-library (www.geobib.lu.se)

245 Linnea Jonsson (2012). Impacts of climate change on Pedunculate oak and Phytophthora activity in north and central Europe

246 Ulrika Belsing (2012) Arktis och Antarktis föränderliga havsistäcken

247 ***Anna Lindstein (2012) Riskområden för erosion och näringsläckage i Segeåns avrinningsområde***

248 Bodil Englund (2012) Klimatanpassningsarbete kring stigande havsnivåer i Kalmar läns kustkommuner

249 Alexandra Dicander (2012) GIS-baserad översvämningskartering i Segeåns avrinningsområde

250 Johannes Jonsson (2012) Defining phenology events with digital repeat photography

251 Joel Lilljebjörn (2012) Flygbildsbaserad skyddszonsinventering vid Segeå

252 Camilla Persson (2012) Beräkning av glaciärers massbalans – En metodanalys med fjärranalys och jämviktslinjehöjd över Storglaciären

253 Rebecka Nilsson (2012) Torkan i Australien 2002-2010 Analys av möjliga orsaker och effekter

254 Ning Zhang (2012) Automated plane detection and extraction from airborne laser scanning data of dense urban areas

255 Bawar Tahir (2012) Comparison of the water balance of two forest stands using the BROOK90 model

256 Shubhangi Lamba (2012) Estimating contemporary methane emissions from tropical wetlands using multiple modelling approaches

257 Mohammed S. Alwesabi (2012) MODIS NDVI satellite data for assessing drought in Somalia during the period 2000-2011

258 Christine Walsh (2012) Aerosol light absorption measurement techniques: A comparison of methods from field data and laboratory experimentation

259 Jole Forsmoo (2012) Desertification in China, causes and preventive actions in modern time

260 Min Wang (2012) Seasonal and inter-annual variability of soil respiration at Skyttorp, a Swedish boreal forest

261 Erica Perming (2012) Nitrogen Footprint vs. Life Cycle Impact Assessment methods – A comparison of the methods in a case study.

262 Sarah Loudin (2012) The response of European forests to the change in summer temperatures: a comparison between normal and warm years, from 1996 to 2006

263 Peng Wang (2012) Web-based public participation GIS application – a case study on flood emergency management

264 Minyi Pan (2012) Uncertainty and Sensitivity Analysis in Soil Strata Model Generation for Ground Settlement Risk Evaluation

265 Mohamed Ahmed (2012) Significance of soil moisture on vegetation greenness in the African Sahel from 1982 to 2008

266 Iurii Shendryk (2013) Integration of LiDAR data and satellite imagery for biomass estimation in conifer-dominated forest

267 Kristian Morin (2013) Mapping moth induced birch forest damage in northern Sweden, with MODIS satellite data

268 Ylva Persson (2013) Refining fuel loads in LPJ-GUESS-SPITFIRE for wet-dry areas - with an emphasis on Kruger National Park in South Africa

269 Md. Ahsan Mozaffar (2013) Biogenic volatile organic compound emissions from Willow trees

270 Lingrui Qi (2013) Urban land expansion model based on SLEUTH, a case study in Dongguan City, China

271 Hasan Mohammed Hameed (2013) Water harvesting in Erbil Governorate, Kurdistan region, Iraq - Detection of suitable sites by using Geographic Information System and Remote Sensing

272 Fredrik Alström (2013) Effekter av en havsnivåhöjning kring Falsterbohalvön.

273 Lovisa Dahlquist (2013) Miljöeffekter av jordbruksinvesteringar i Etiopien

274 Sebastian Andersson Hylander (2013) Ekosystemtjänster i svenska agroforestrysystem

275 Vlad Pirvulescu (2013) Application of the eddy-covariance method under the canopy at a boreal forest site in central Sweden

276 Malin Broberg (2013) Emissions of biogenic volatile organic compounds in a Salix biofuel plantation – field study in Grästorp (Sweden)

277 Linn Renström (2013) Flygbildsbaserad förändringsstudie inom skyddszoner längs vattendrag

278 Josefin Methi Sundell (2013) Skötseleffekter av miljöersättningen för natur- och kulturmiljöer i odlingslandskapets småbiotoper

279 Kristín Agustsdottír (2013) Fishing from Space: Mackerel fishing in Icelandic

waters and correlation with satellite variables

280 Cristián Escobar Avaria (2013) Simulating current regional pattern and composition of Chilean native forests using a dynamic ecosystem model

281 Martin Nilsson (2013) Comparison of MODIS-Algorithms for Estimating Gross Primary Production from Satellite Data in semi-arid Africa

282 Victor Strevens Bolmgren (2013) The Road to Happiness – A Spatial Study of Accessibility and Well-Being in Hambantota, Sri Lanka

283 Amelie Lindgren (2013) Spatiotemporal variations of net methane emissions and its causes across an ombrotrophic peatland - A site study from Southern Sweden

284 Elisabeth Vogel (2013) The temporal and spatial variability of soil respiration in boreal forests - A case study of Norunda forest, Central Sweden

285 Cansu Karsili (2013) Calculation of past and present water availability in the Mediterranean region and future estimates according to the Thornthwaite water-balance model

286 Elise Palm (2013) Finding a method for simplified biomass measurements on Sahelian grasslands

287 Manon Marcon (2013) Analysis of biodiversity spatial patterns across multiple taxa, in Sweden

288 Emma Li Johansson (2013) A multi-scale analysis of biofuel-related land acquisitions in Tanzania - with focus on Sweden as an investor

289 Dipa Paul Chowdhury (2013) Centennial and Millennial climate-carbon cycle feedback analysis for future anthropogenic climate change

290 Zhiyong Qi (2013) Geovisualization using HTML5 - A case study to improve animations of historical geographic data

291 Boyi Jiang (2013) GIS-based time series study of soil erosion risk using the Revised Universal Soil Loss Equation (RUSLE) model in a micro-catchment on Mount Elgon, Uganda

292 Sabina Berntsson & Josefin Winberg (2013) The influence of water availability on land cover and tree functionality in a small-holder farming system. A minor field study in Trans Nzoia County, NW Kenya

293 Camilla Blixt (2013) Vattenkvalitet - En fältstudie av skånska Säbybäcken

294 Mattias Spångmyr (2014) Development of an Open-Source Mobile Application for Emergency Data Collection

295 Hammad Javid (2013) Snowmelt and Runoff Assessment of Talas River Basin Using Remote Sensing Approach

296 Kirstine Skov (2014) Spatiotemporal variability in methane emission from an Arctic fen over a growing season – dynamics and driving factors

297 Sandra Persson (2014) Estimating leaf area index from satellite data in deciduous forests of southern Sweden

298 Ludvig Forslund (2014) Using digital repeat photography for monitoring the regrowth of a clear-cut area

299 Julia Jacobsson (2014) The Suitability of Using Landsat TM-5 Images for Estimating Chromophoric Dissolved Organic Matter in Subarctic Lakes
300 Johan Westin (2014) Remote sensing of deforestation along the trans-Amazonian highway
301 Sean Demet (2014) Modeling the evolution of wildfire: an analysis of short term wildfire events and their relationship to meteorological variables
302 Madelene Holmblad (2014). How does urban discharge affect a lake in a recreational area in central Sweden? – A comparison of metals in the sediments of three similar lakes
303 Sohidul Islam (2014) The effect of the freshwater-sea transition on short-term dissolved organic carbon bio-reactivity: the case of Baltic Sea river mouths
304 Mozafar Veysipanah (2014) Polynomial trends of vegetation phenology in Sahelian to equatorial Africa using remotely sensed time series from 1983 to 2005
305 Natalia Kelbus (2014) Is there new particle formation in the marine boundary layer of the North Sea?